

AD-A143 647

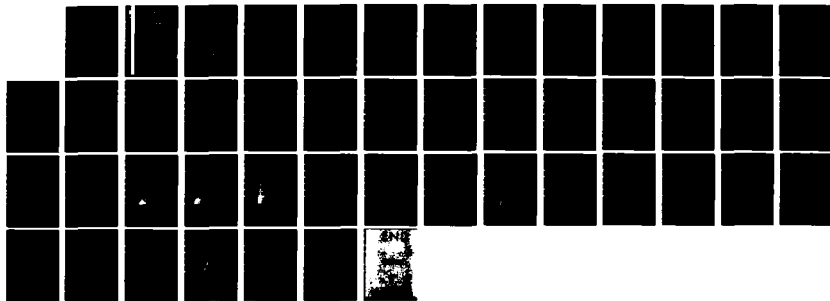
THE CALCULATION OF THE RADAR VERTICAL COVERAGE DIAGRAM
(U) ROYAL AUSTRALIAN NAVY RESEARCH LAB EDGECLIFF
M R BATTAGLIA MAY 84 RANRL-T/NOTE(EXT)-1/84

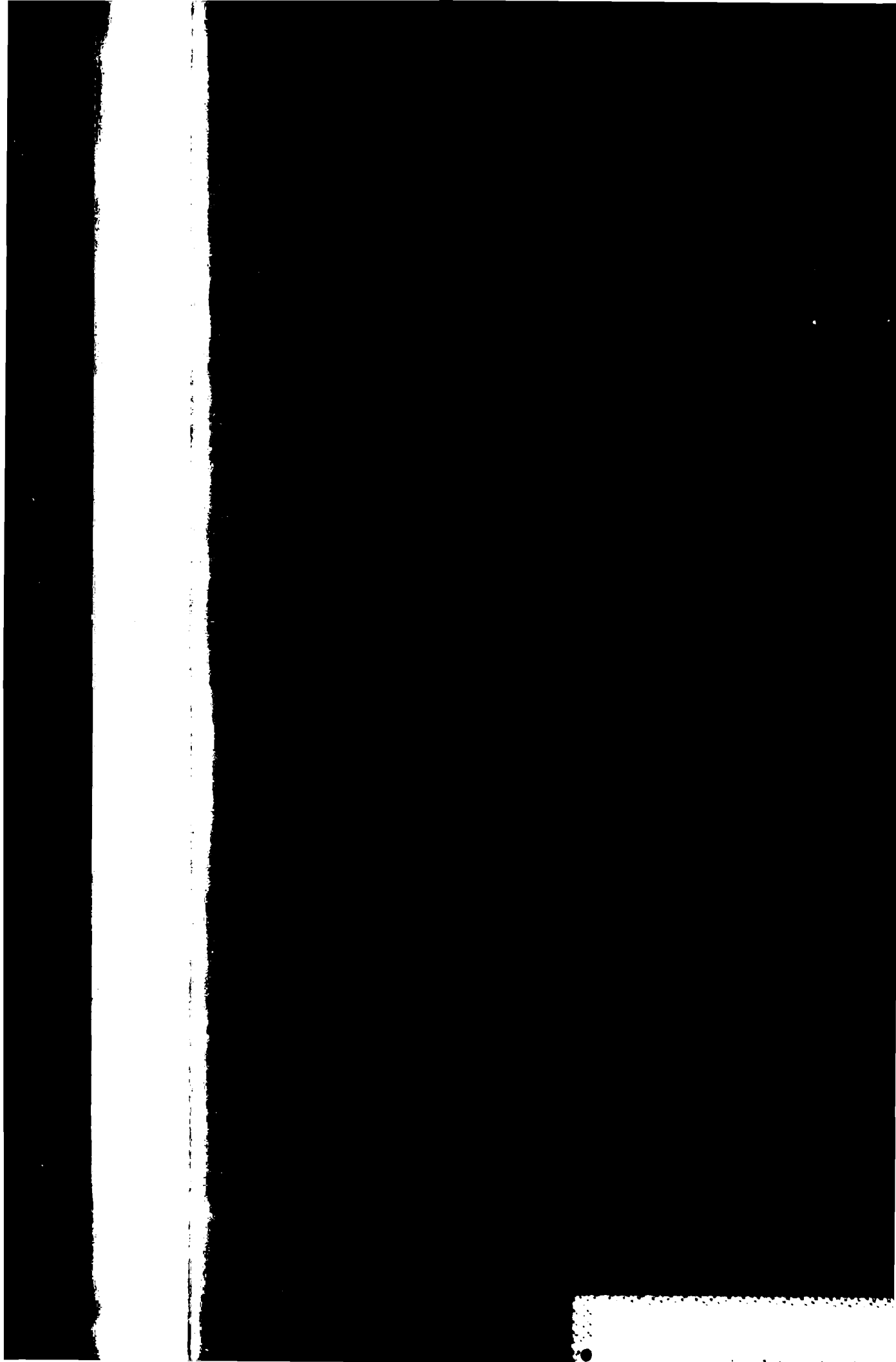
1/1

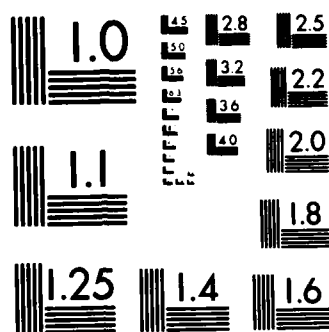
UNCLASSIFIED

F/G 17/9

NL







MICROCOPY RESOLUTION TEST CHART
NATIONAL BUREAU OF STANDARDS-1963-A

12

UNCLASSIFIED

UNCLASSIFIED

RANRL T/Note (Ext)-1/84 ✓

AR Number: AR003-419

AD-A143 647



DEPARTMENT OF DEFENCE
DEFENCE SCIENCE AND TECHNOLOGY ORGANISATION
R.A.N. RESEARCH LABORATORY
EDGECLIFF, N.S.W.

RANRL TECHNICAL NOTE
(External) No 1/84

THE CALCULATION OF THE RADAR VERTICAL
COVERAGE DIAGRAM

DTIC FILE COPY

M.R.BATTAGLIA

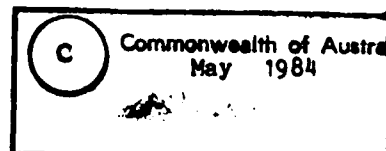
THE UNITED STATES NATIONAL
TECHNICAL INFORMATION SERVICE
IS AUTHORISED TO
REPRODUCE AND SELL THIS REPORT

APPROVED FOR PUBLIC RELEASE

DTIC
ELECTE
JUL 31 1984
S
E

COPY No. 1

UNCLASSIFIED



UNCLASSIFIED

84 07 31 024

UNCLASSIFIED

DEPARTMENT OF DEFENCE
R.A.N. RESEARCH LABORATORY



© Commonwealth of Australia (1984)

RANRL TECHNICAL NOTE (EXTERNAL) No 1/84

THE CALCULATION OF THE RADAR
VERTICAL COVERAGE DIAGRAM



M.R.BATTAGLIA



Accession For	
NTIS GRA&I	<input checked="" type="checkbox"/>
DTIC TAB	<input type="checkbox"/>
Unannounced	<input type="checkbox"/>
Justification	
By	
Distribution/	
Availability Codes	
Dist	Avail and/or Special
A-1	

ABSTRACT

Algorithms are described for the calculation and plotting of radar vertical coverage diagrams. Two contour VCD algorithms are presented, with a brief discussion on the problem of numerical stability, and the effects of ship motion and frequency agility.

POSTAL ADDRESS: The Director, RAN Research Laboratory
P.O. Box 706 Darlinghurst, N.S.W. 2010

UNCLASSIFIED

CONTENTS

1. INTRODUCTION	1
2. THE RADAR EQUATION	1
3. REQUIRED SIGNAL-TO-NOISE	2
3.1 Approximate Formulae	2
3.2 Iterative Solutions	4
4. THE RADAR VCD	4
4.1 VCD Envelope	5
4.2 The Roughness Factor	6
4.3 Antenna Pattern Functions	7
5. GRAPHICAL REPRESENTATION OF VCD	7
6. CONTOUR PLOTTING	8
6.1 Asymptotic Behaviour - The flat Earth Limit	8
6.2 Spherical Earth Model	9
6.3 Description of Main Program	10
7. EFFECT OF SHIP MOTION	12
8. FREQUENCY AGILITY AND DIVERSITY	14
ACKNOWLEDGEMENTS	14
REFERENCES	15
LIST OF ANNEXES	
A Calculation of Threshold for Fixed Threshold Detectors	16
B Calculation of Paint Probability for Marcum, Swerling and Weinstock Targets	17
C Calculation of Required Signal-to-Noise	18
D Calculation of Paint Probability for Non-fluctuating Targets	19
E Main Program for Contour VCD Calculations	20
DISTRIBUTION	42
DOCUMENT CONTROL DATA SHEET	43

1. Introduction

Operational performance of Naval radars is routinely checked by measurement of the vertical coverage diagram (VCD). Comparisons of returns from a calibrated target with the VCD facilitates the detection of any degradation. This may be in the form of a lower average detection range or 'holes' in the vertical coverage. The former may result from electronic degradation or transmission line losses, while the latter may result from antenna damage or multipath effects - these being determined by sea state and choice of antenna height or operating frequency.

In reference 1, computer programs were described which calculated (i) the radar return from a target flying a specified height/range profile and (ii) the probability of paint for fluctuating and non-fluctuating targets. Refinements to the model, and the theoretical basis of the algorithms were outlined in reference 2.

Comparisons have been made between the output of these programs and the measured returns in the RAN sphere drop calibration trials. In the absence of ducting, any differences can generally be attributed to plumbing or other isotropic losses.

RANRL has been requested (ref 3) to produce programs suitable for desktop computers to solve the inverse problems - (i) the calculation of signal-to-noise required to yield a given probability of paint and (ii) the calculation and plotting of detection contours in a multipath environment. The ensuing sections describe the algorithms used in the programs.

2. The Radar Equation

The power returned in free space from a target of cross-section σ is given by the monostatic radar equation

$$P_r = \frac{P_t G^2 \lambda^3 \sigma}{(4\pi)^3 R^4} \quad 1.$$

where P_t is the transmitted power, G is the power gain, λ is the radar wavelength and R is the target range. Multipath, diffraction and other environmental effects are accounted for by the pattern propagation factor (F) and the atmospheric loss factor (L)

$$P_r = \frac{P_t G^2 \lambda^3 \sigma F^4}{(4\pi)^3 R^4 L} \quad 2.$$

The problem addressed in this paper is the calculation of R in equation 2, which may be recast to provide an expression for the maximum single-blip detection range:

$$R_{\max} = \left[\frac{P_t C^2 \lambda^2 \sigma}{(4\pi)^3 P_n D_0 L} \right]^{0.25} \quad 3.$$

where P_t is the peak transmitted power and P_n is the system noise power. D_0 is the single-pulse signal-to-noise ratio required to yield the desired probability of paint for a given number of pulses integrated, false alarm rate and target return statistics. In the absence of clutter, the limit to signal detectability is governed by the pulse energy, so that the effective noise power P_n , referred to the antenna, is determined by the transmitted pulse width (τ), the antenna noise temperature (T_a), the receiving line losses (L_r) and the receiver noise figure (NF)

$$P_n = k/\tau \left[T_a + T_r(L_r-1) + L_r T_o(NF-1) \right] \quad 4.$$

where T_r and T_o are the temperature of the receiving line and 290 K respectively, and k is Boltzmann's constant. If the receiver noise bandwidth B_n is used instead of $1/\tau$ in (4) the transmitted power should be multiplied by $B\tau$, the time-bandwidth constant, to give the effective S/N for probability of detection calculations. If clutter-to-noise is near unity, it is convenient to assume that the clutter-plus-noise variable ($P_c + P_n$) has the same statistical distribution as receiver noise, and this Rayleigh distributed total noise power is used for P_n in equation 3.

3. Required Signal-to-Noise

3.1 Approximate Formulae

There are numerous approximate formulae in the radar literature for evaluating paint probability from S/N (and vice versa). Reasonable estimates of detection range can be obtained using the simple formula suggested by Neuvy (ref 4):

$$D_0 = 10 \log \left[\frac{\alpha}{N^\gamma} \cdot \frac{\log PFA}{(\log(1/P_d))^\beta} \right] \quad 5.$$

where PFA is the probability of false alarm, P_d is the probability of paint, N is the number of pulses incoherently integrated. The detector law is described by the 'constant' γ which is often given the empirical value of 2/3 (ref 5) rather than the asymptotic limit of 1/2. Neuvy has given heuristic estimates of α and β for the Swerling and Marcum (non-fluctuating) targets as shown in Table 1.

Case	c	β
Swerling I	$2/3[1 + 2/3 \exp(-N/3)]$	1
II	1	$1/6 + \exp(-N/3)$
III	$3/4[1 + 2/3 \exp(-N/3)]$	2/3
IV	1	$1/6 + 2/3 \exp(-N/3)$
Non-fluctuating	$1 + 2 \exp(-N/3)$	1/6

Table 1. Neuwy parameters for Marcum and Swerling targets.

N	Swerling Case				Eqn (6)
	I	III	II	IV	
1	10.5924	10.3747	10.5924	10.3747	10.5924
2	8.1681	7.9547	7.9547	7.9295	7.9547
3	6.8091	6.5984	6.5735	6.5938	6.7176
4	5.8732	5.6644	5.6443	5.6807	5.6060
5	5.1639	4.9565	4.9478	4.9907	4.8528
6	4.5949	4.3888	4.3926	4.4380	4.2808
7	4.1213	3.9163	3.9320	3.9781	3.8188
8	3.7165	3.5123	3.5392	3.5851	3.4310
9	3.3636	3.1601	3.1972	3.2425	3.0968
10	3.0511	2.8483	2.8947	2.9391	2.8030
20	1.0674	0.8689	0.9763	1.0105	0.9560
30	-0.0397	-0.2360	-0.0962	-0.0687	-0.0798
40	-0.8042	-0.9989	-0.8384	-0.8153	-0.8024
50	-1.3861	-1.5798	-1.4045	-1.3845	-1.3574
60	-1.8550	-2.0479	-1.8613	-1.8437	-1.8079
70	-2.2471	-2.4393	-2.2438	-2.2280	-2.1871
80	-2.5837	-2.7754	-2.5726	-2.5583	-2.5143
90	-2.8785	-3.0697	-2.8608	-2.8476	-2.8021
100	-3.1405	-3.3312	-3.1171	-3.1049	-3.0590
200	-4.8285	-5.0169	-4.7736	-4.7666	-4.7370
300	-5.7918	-5.9791	-5.7225	-5.7175	-5.7111
400	-6.4664	-6.6531	-6.3883	-6.3844	-6.3996
500	-6.9853	-7.1715	-6.9012	-6.8980	-6.9324
600	-7.4065	-7.5925	-7.3180	-7.3153	-7.3670
700	-7.7611	-7.9467	-7.6691	-7.6667	-7.7340
800	-8.0672	-8.2526	-7.9723	-7.9702	-8.0516

Table 2. Required signal-to-noise (dB) tabulated for N=1 to 800 pulses integrated (PFA=0.000001, $P_d=0.33$).
Iterative solutions (columns 2-5) used fitted data in column 6 as 'first guess'.

These formulae are accurate to within a few dB for $0.1 < P_d < 0.9$ and moderate values of N . This range is not adequate since (i) the 95% contour is often specified as the required detectability contour and (ii) cumulative paint probability considerations might warrant the plotting of a $P_d < 10\%$ contour. The formulae also do not give good agreement for $1 < N < 5$ which is typical for 3-D radar, nor are they applicable to very slowly fluctuating (Weinstock) targets. Expressions of comparable accuracy have been given by Albersheim (ref 6) and Blake (ref 7) for non-fluctuating targets.

3.2 Iterative Solutions

The formulae described above are not valid over a sufficiently large range of P_d , N , PFA and target scintillation rate to be used for routine VCD calculations, but are sometimes useful in providing a starting point for an iterative algorithm. However, in the unreliable regions (such as moderately large N and $P_d > 90\%$) numerical instability poses a serious problem. A more robust starting point is required which covers the range of radar and target parameters likely to be encountered.

The method used here is based on the observation that D_0 , for 33% probability of detection in gaussian noise, is virtually independent of the amplitude statistics of the target (see figure 1). Regression analysis of D_0 data for $P_d = 0.33$, $3 < N < 1000$, $PFA = 10^{-6}$, Swerling case II, and non-coherent integration yields the following result

$$D_0 = 7.138 + 1.018/\log(N) - 5.533.\log(N) \quad 6.$$

with D_0 in dB. Values for $N=1$ and 2 are evaluated separately in the program.

The secant iterative method with equation 6 as first guess, together with the algorithms of reference 2, were used to produce the data in table 2. Iteration was stopped at $P_d = 0.33 \pm 0.00001$. The accuracy of equation 6 is of the order of the dependence on target scintillation (± 0.1 dB) at 33% probability of detection. Results for 50% and 95% ($\pm 0.001\%$) are shown in graphical form in figures 2 and 3.

4. The Radar VCD

In free space, the detectability contour, or vertical coverage diagram, is determined by equation 3 with F replaced by the antenna pattern function $f(\theta)$

$$R_{\max} = f(\theta).R_0 \quad 7.$$

where R_0 is the detection range along boresight, and θ is the elevation

angle. This smoothed contour is also useful for estimating mean detection ranges at higher elevation angles and moderate sea states, in which case the multipath structure is washed out (see also later section on ship motion). At lower elevation angles, or sea states, multipath lobing must be considered and the detection contour becomes

$$E_{\max} = F \cdot E_0 \quad 8.$$

Under non-ducting conditions, the pattern propagation factor, F in the interference region is

$$F = f(\theta_1) \cdot \sqrt{1 + x^2 + 2x \cos \theta} \quad 9.$$

and may take values between 0 and 2. The phase difference θ is the sum of contributions from the geometric path difference between the direct and indirect rays (fig 4), and the phase difference on reflection from the sea surface of the indirect ray. The reflectivity parameter x is

$$x = \frac{r \rho D f(\theta_2)}{f(\theta_1)} \quad 10.$$

in which D is the divergence factor, r is the roughness factor, ρ is the dielectric reflectivity (the reflectivity which would apply if the sea were perfectly smooth) and θ_1 and θ_2 are as shown in figure 4.

For elevation angles near the horizon, and for targets over the horizon, F is calculated using diffraction theory (or by interpolation as described in ref 1) with

$$F = f(\theta_1) \cdot \sqrt{U(X) \cdot V(Z_1) \cdot V(Z_2)} \quad 11.$$

where X , Z_1 , Z_2 are range, target height and antenna height respectively in natural units and the functions V and U are gain functions described in reference 2.

4.1 VCD Envelope

The main features of the VCD for Naval radars can be calculated using ray theory. The envelope of E_{\max} is obtained with equations 8 and 9 with

$$\theta_{\max} = 2\pi m \quad (m=1,2,3,\dots) \quad 12.$$

so that,

$$E_{\max}(\text{envelope}) = f(\theta_1) \cdot (1+x) \cdot E_0 \quad 13.$$

Within the range of elevation and grazing angles of interest, the shape of the VCD is thus dominated by $f(\theta)$ and r .

4.2 The Roughness Factor

The reflectivity of the indirect ray can be written as

$$\Gamma = r \cdot \rho \cdot e^{-j\theta} \quad 14.$$

where r is the roughness factor, and ρ and θ are the magnitude and phase respectively of the specular reflection coefficient. Formulae for ρ and θ as functions of grazing angle, frequency, water temperature and salinity are given in reference 2 and are in good agreement with experimental data. The dependence of the roughness factor on grazing angle and frequency is less straightforward, and there is a paucity of experimental data.

Ament (ref 8) has shown that if the wave height distribution is gaussian, (variance σ^2), then the surface roughness will also be gaussian

$$r = e^{-2s^2} \quad 15.$$

where

$$s = 2\pi\sigma \cdot \sin\gamma / \lambda \quad 15a.$$

This equation gives good agreement at low grazing angles (γ), but this is to be expected since $r \rightarrow 1$ as $\gamma \rightarrow 0$. That is, most models will predict $\Gamma_{\max} \sim 2R_0$ for the lowest multipath maximum over a wide range of frequencies and sea states, despite the lack of agreement for the high altitude coverage.

At higher values of s the reflection is not purely specular. The additional diffuse component adds to the fluctuation in the pattern propagation factor, but not to its average value. The random component of F is not considered in the program, but rather an effective constant value is assumed. Reasonable agreement for large s is obtained using the empirical expression given in reference 1:

$$\begin{aligned} r &= e^{-2s^2} && \text{for } r > 0.44 && 16. \\ &= e^{-1.2732s} && r \leq 0.44 \end{aligned}$$

The program also makes use of the Burling relationship between significant wave height ($H_{1/3}$) and σ

$$H_{1/3} = 4 \sigma \quad 17.$$

4.3 Antenna Pattern Functions

At high elevation angles and moderate sea states $x \rightarrow 0$ and the envelope of $E_{\text{ra}\lambda}$ is dominated by the APF, as per eqn 7. Elsewhere, the antenna pattern function of both the direct and indirect rays are required for the calculation of E . In general, the APF needs to be represented adequately out to the first sidelobe. The program calculates either (i) a cosecant-squared pattern or (ii) a modified $\sin u/\lambda$ fan beam of the form

$$f(\theta) = \frac{\sin \pi \sqrt{u^2 - B^2}}{\pi \sqrt{u^2 - B^2}} \quad 18.$$

where $u = d \cdot \sin \theta / \lambda$ and B is a constant for the antenna, which describes the sidelobe level and aperture efficiency. Methods for calculating B from the sidelobe level are described in reference 2

5. Graphical Representation of VCD

In the absence of pitch and roll the VCD is independent of radar azimuth (neglecting blind arcs and superstructure multipath) so that the VCD can be displayed as a 2-D graphical representation. Variations with range and height of paint probability or signal-to-noise can be described by an arbitrary number of grey scales.

In figures 5-8, the VCD of a UHF air search radar and a G-band surface search radar are illustrated for two sea states. Gross parameters used for the UHF radar are $\lambda = 0.7$ metre, antenna height $h_1 = 30$ metre, $N=75$ pulses incoherently integrated, sea states 0 and 6, and a free space range of $E_0 = 80$ n.miles against a 1 metre-squared target. Parameters used for the G-band radar are $\lambda = 0.05$ metre, $h_1 = 25$ metre, $N = 5$, sea states 0 and 3 and $E_0 = 17$ n.miles. Standard atmospheric conditions and scan-to-scan (Swerling case I) target scintillation are assumed. The grey scales correspond to paint probability regions $P > 95\%$, $50\% < P < 95\%$, $5\% < P < 50\%$ and $P < 5\%$, and were computed as described in the previous section.

The VCD's were produced by taking 120 cuts in height for 200 range increments. Sea clutter was included in the noise calculations, using the expressions described in reference 2. For reasons of clarity the plots are not truncated at minimum range and maximum unambiguous range as determined by the radiated pulse width and PRF respectively. In order to resolve the structure in the G-band plots, calculations were carried out only to 4000 feet and limited to sea state 3, while the UHF calculations

were carried out to a height sufficient to contain the 5% probability contour.

The calculations for figures 5-8 took a few minutes of processing time on a CDC Cyber 76 mainframe computer. Such a program is however unsuitable for small desktops, such as the Tektronix Graphics System specified in reference 3, since similar calculations would take 2-3 days of computer time for each plot. The next section describes methods for producing line contour VCD's which can be quickly computed on a small desktop machine, using a modification of the program described in ref 1.

6. Contour Plotting

6.1 Asymptotic Behaviour The Flat Earth Limit

Fast algorithms for computing contour VCD's are not easily implemented due to the lack of symmetry in the multipath lobing structure. One method often employed is to perform an approximate calculation of the VCD using the flat earth multipath results and to modify the computed results graphically or by scaling to account for curvature. Even this approach however will not be generally applicable due to the additional geometric approximations that must be made.

In the flat earth limit $D \rightarrow 1$ and, for horizontally polarized UHF radars at low to moderate elevation angles, $r=1$ and the phase difference on reflection is π radians. The path difference between direct and indirect rays for a target at ground range G is

$$\delta = \sqrt{(h_1 + h_2)^2 + G^2} - \sqrt{(h_2 - h_1)^2 + G^2}$$

If the free space range of the radar is large compared with the sum of target and antenna heights the path difference for constructive interference is given approximately as

$$\delta = \frac{2h_1 h_2}{R \cos \theta} \quad 19.$$

Within the antenna main lobe ($f(\theta) \sim 1$) the pattern propagation factor then simplifies as

$$\begin{aligned} F &= 2 \left[\sin(2\pi h_1 h_2 / \lambda G) \right] \\ &= 2 \left[\sin \frac{2\pi h_1}{\lambda} \left(\tan \theta + \frac{h_1}{G} \right) \right] \quad 20. \end{aligned}$$

Usually $G \gg h_1 / \tan \theta$ for naval search radars at ranges of interest, so that the VCD's produced from the flat earth model are highly symmetric - that is, only one calculation of multipath geometry need be performed for one range at each elevation angle increment, with R^{-4} scaling to determine the range for a specified probability of detection and false alarm rate (using the algorithms of section 3). A first order correction for the effect of the earth's curvature can be included after the last approximation. This is equivalent to assuming that the sea surface is flat up to the point of reflection so that the final result requires only the transformation $h_2 \rightarrow h_2 + G^2 / 2a_e$.

The algorithms used in the program described here do not rely on the flat earth model, however the gross structure of the VCD can be determined using the procedure described above. Such a description is therefore a useful basis for a more general algorithm.

6.2 Spherical Earth Model

- Dependence of F on Range

The flat earth model predicts that the lobe maxima for long range naval radars occur (with $F=2$) at elevation angles

$$\theta_{\max} = \sin^{-1} (2m-1)\lambda / 4h_1 \quad m=1,2,3,\dots \quad 21.$$

It is clear from figures 5-8 that, in the more general model, $F=2$ at the lobe maxima only at low elevation angles. This implies, not only that twice the free space range will be achieved only at lower altitude, but also that the lobe spacing is not uniform. Equation 21 is, however, useful for determining the elevation angle spacing required to fully resolve the multipath structure. In the program, ten points are calculated per nominal lobe spacing. This facilitates both resolution of the lobes and the ability to read the radar range from the plots to a within a few percent of R_0 .

The behaviour at constant elevation angle for a spherical earth is most easily demonstrated graphically. Figures 9 and 10 are typical plots of the signal return for the UHF radar described in the previous section. The plots are for a 1 metre-squared target at two intermediate elevation angles, separated by half a nominal lobe spacing, at sea states 0 and 6. If the free space range of the radar is large compared with the clutter horizon, algorithms for contour VCD's are likely to be most stable at higher sea states due to the reduced multipath lobing. This is seen in the plot for sea state 6 (figure 10) where results for both elevation angles yield results which are close to the free space result. Since the power return decays as the fourth power of range, either a scaling or iterative algorithm should calculate the required

signal-to-noise in one or two iterations even if the first is inaccurate.

The behaviour at low sea states is less well behaved and robust algorithms are generally required. In figure 9 the results at the free space range (80 n.miles) is qualitatively different for two elevation angles selected. One curve corresponds to the position of a lobe maximum (at 80 n.miles) and R^{-4} behaviour is seen. The other curve is 2.0 times the free space range. This type of behaviour is not unexpected and implies that as long as the first guess for range is not too far from the free space range, the detection range ($S/N = \Gamma_0$) maxima will generally be easily computed. At very short ranges, range hopping occurs for constant elevation angle calculations so that iterative algorithms may be numerically unstable.

As a corollary, iterative algorithms may be unsuitable for range search radars such as the G-band radar of the previous section. In the worst case there may be either no solution or several solutions for $S/N = \Gamma_0$ at a given elevation angle. The former case may arise at low sea states if the detection range is of the order of the clutter range while the latter will be worst at low sea states where range lobe lobing is most pronounced.

6.3 Description of Main Program

Either of two algorithms may be selected in the main program. In cases where numerical stability is not a problem the preferred algorithm is an iterative search method. This algorithm gives reliable results at moderate sea states for naval radars where the detection range is large compared with the clutter horizon. This method requires that there is a solution along a selected elevation angle and that the power is reasonable (power monotonically decreasing with range). The detection range can be calculated with arbitrary precision. A sensitivity of 0.25 dB should be acceptable for most applications. 10 points are plotted per nominal lobe spacing.

In order to increase the probability of the search algorithm finding a numerically stable region, the first two corrections to the range are scaled assuming R^{-4} and R^{-6} decay law respectively (to reduce ringing), with subsequent iterations independent of the decay law. If a solution has not been obtained by a specified number of iterations, the 'solution' plotted will correspond to the minimum value of the power. This method will therefore produce reliable ranges in the main lobe but not necessarily in the nulls. This loss of

of little consequence (see figures 5-8) especially considering that the power in the nulls is highly variable due to ship motion (discussed in next section), wave height fluctuations, atmospheric inhomogeneity, and other factors.

The second algorithm is a one-step scaling algorithm, so that the computed detectability range, at a specified elevation angle, will in general be reliable only if the first guess is close to the actual detectability range. The scaling algorithm in the program is optimized to produce a reliable envelope for VCD contour since the first guess at any elevation angle is the range to the lobe maximum, given by equation 13. Since the reflectivity parameter x is a function of R , it is not known until the final solution is obtained. An estimate \hat{x} is used, and this provides an estimate \hat{R}_{\max} :

$$\hat{R}_{\max} = R_0 f(\theta) \cdot (1 + \hat{x}_i) \quad 22.$$

The estimate \hat{x}_i is the value corresponding to the last solution (x_{i-1}). With this procedure, R_{\max} will be calculable to within a few percent at sea state 0 if at least 10 points are calculated per multipath lobe. At higher elevation angles and/or sea states the multipath lobing structure is washed out ($x_i \rightarrow 0$) so that this algorithm will be both robust and accurate if R_0 is greater than the clutter horizon.

Plots using these algorithms are given in plots 11-17. The contour selected is 0 dB in all cases, which corresponds to 4% and 52% probability of paint for the G-band ($N=5$) and UHF ($N=75$) radars respectively against a Swerling case I, 1 metre-squared target. Figures 11 and 12 used the iterative algorithm (0.25 dB sensitivity) at sea states 0 and 6. The contour VCD's are in good agreement with the grey scale envelopes of figures 5 and 6. An additional plot for sea state 3 (fig 13) is included to illustrate the gradual, and very significant, decrease in maximum height with sea state. The same parameters were used to produce the plots in figures 14 and 15 with the scaling algorithm. Although this algorithm is optimized at the lobe maxima, it also gives good agreement in the mid-lobe region. The lower half of each lobe is generally well reproduced to much shorter ranges - this is fortuitous since this is the lobe region of interest for inbound air targets.

Figure 16 and 17 show the results of the scaling algorithm for the G-band contours, with the calculations stopped at an elevation angle corresponding to the maximum height in the full graphical representations (fig 7-8). Again, the 0 dB contour (4%) is consistent with the 5% grey

scale envelope of figures 7-8. With this radar, the pattern propagation factor has a stronger range-dependence so that the iterative algorithm is numerically less stable. The manifestation of this is a VCD with a much higher incidence of 'bad' data points (about 5% of all points calculated). At sea state 0, the lobes for this radar are pronounced but closely spaced so that only the envelope of the VCD contour is easily measured (sufficient reason for using the quicker scaling method). At higher sea states the effect of ship motion further complicates the VCD.

7. Effect of Ship Motion

The motion of the ship is most conveniently described in terms of the reference axes systems defined in figure 18. A natural choice for the 'space-fixed' axis system utilizes the mean sea surface as the x-y plane. The ship's axis system is also naturally defined by the effective plane of symmetry through the keel, which is defined as the x'-z' plane, with the y'-axis passing through the antenna.

Relative motion of the two axes systems about the vertical (yaw) is equivalent to a fluctuation in the antenna rotation rate and, thus, the number of pulses integrated. Similarly, the number of hits per scan is increased or decreased during a rapid turn. Although this motion may be of the same order as the normal antenna motion, the probability of detection is only a weak function of the number of pulses incoherently integrated, and can therefore be ignored in most cases. Motion of the ship in the x-y plane is also ignored since the VCD is plotted in terms of relative range which will not change significantly during the time on target for normal antenna rotation rates and target range rates.

Pitch and roll can be defined as the angles θ and ϕ respectively in figure 18. The effects of ship 'rotation' are symmetric in pitch and roll unless a specific target bearing is considered. For a target on the bow, pitch has the same effect as varying the antenna tilt in the x,y,z axis system while preserving the polarization of the radiation. (The effect of the vertical motion of the antenna during pitch/roll is discussed later in the section on heave). Pitch or roll can be significant compared with vertical beamwidth, even for wide beamwidth search radars. This not only has the effect of increasing the maximum angle of the main antenna lobe VCD, but also gives rise to calculable fluctuations in the pattern propagation factor at moderate elevation angles due to variations in the APF of the direct and indirect

rays. This is shown in figure 19, where the antenna tilt was allowed to vary randomly between zero and 10% of the vertical beamwidth.

The effect of roll for a target along zero relative bearing also has a small azimuth-fluctuation effect for targets at moderate elevation angles. (This effect is not normally significant, or else it would provide an elegant method of determining target elevation using a 2-D radar.) A second effect for this relative geometry is that polarization of the radiation in the space-fixed system is partially converted to the opposite sense. The detecting antenna is only concerned with the polarization in the ship's axis system, so that this is only manifested through multipath effects. Six degrees of roll converts only 1% of the radiation to the opposite polarization. At grazing incidence for the indirect ray, the phase difference and reflectivity are near π and 1 respectively for both polarizations, so that the lowest lobe is virtually independent of polarization. At moderate elevation, the magnitude and phase for vertical polarization may be sufficiently different to put maxima at the elevation angle of a minimum for the opposite polarization. Since the detection range is of the order of $(S/N)^{0.25}$, the nulls for a 1% polarization change may be filled to about a third of the range for the adjacent lobe maxima.

In the case of heave, the effect is simply related to the ratio of heave to mean antenna height above sea level. A simulation of the effect of heave is shown in figure 20 (one run only), where the antenna height was uniformly distributed over the nominal heave dimension. The effect on the lower lobes is only slight, but heave has the effect of filling in the upper lobes and thus reducing the mean detection range along a lobe maximum. If the mean of many simulation runs is calculated for each elevation angle, the nulls at the n -th lobe will be completely filled if n is of order (antenna height/2.heave) or greater, decreasing in effect with decreasing elevation angle.

Ship heave will also affect the probability of detection by its effect on the target fluctuation statistics. In the case of slowly fluctuating (Weinstock) targets, heave will modify the scintillation to scan-to-scan (Swierling case I) at higher elevation angles but will have a reduced effect on the amplitude statistics at lower angles. Targets with Swierling case I-IV statistics will not be affected to the same extent since ship motion is negligible on a pulse-to-pulse timescale for typical PRF's.

8. Frequency Agility and Diversity

The radars discussed above are assumed to have a transmitted frequency bandwidth of order of the inverse of the pulsewidth - typically 1 MHz. With pulse compression radar it is the inverse of the compressed pulsewidth. In addition, the centre frequency may be tuned over a range of several percent - typically tens of MHz. The single-pulse bandwidth is small compared with the centre frequency, and so has no significant effect on the VCD, while the tunability of the radar set simply changes the number of lobes that fit into the antenna main lobe at fairly long time intervals. (The frequency term in the radar equation can be assumed to be a constant, since the detection range varies as the square root of the wavelength.)

Frequency agility has an analogous effect on the radar VCD. The detectability, averaged over all transmitted frequencies, may be the same as a simple tunable radar, however on a scan-to-scan timescale the radar VCD's are quite different. The elevation angle to the n -th lobe is approximately proportional to the ratio of the transmitted wavelength to the antenna height. If the agility was random, and on a scan-to-scan basis, the effect on the VCD would be similar to the heave simulation in figure 20. That is, the lower lobes would be unaffected but the power in the upper lobes would be fluctuating about the free space level. Pulse-to-pulse random agility yields the same mean detection range but the fluctuations are averaged out in the integration process. A second effect of random pulse-to-pulse frequency agility is on the number of independently fading signal groups per scan, or alternately the number of degrees of freedom of the equivalent Chi-square target. If F frequencies are transmitted per scan with sufficient separation to have independent echoes, then a target which is represented as having $2K$ degrees of freedom for the fixed frequency radar has up to $2KF$ degrees of freedom for the pulse-to-pulse frequency agile radar ($K=F, N, 2F$ and $2N$ for Swerling cases I, II III and IV respectively).

Acknowledgement.

Helpful suggestions from LtCdr P Williams are acknowledged.

REFERENCES

1. Battaglia, M.R. (1983). RAN Research Laboratory. A Computer Program for the Prediction of Search Radar Performance. (U) RANRL Tech Note (Ext) 1/83. UNCLASSIFIED.
2. Battaglia, M.R. and P.Williams (1983). RAN Research Laboratory. A Model of Radar Propagation and Detection.(U) RANRL Tech Note (Ext) 2/83. UNCLASSIFIED.
3. RANTAU Minute 59-17-2 (DS) , 7th Sept 1983 (R).
4. Neuvy, J. (1970) 'An Aspect of Determining the Range of Radar Detection', I.E.E.E. Trans on Aerospace and Electronic Systems, AES-6 (4), p 514.
5. Brookner, E (Ed) (1977). Radar Technology, Artech, Dedham, p 387.
6. Tufts, D.W. and A.J.Cann (1983). 'On Albersheir's Detection Equation', I.E.E.E. Trans on Aerospace and Electronic Systems, AES-19 (4), p 643.
7. Blake, L.V. (1980). Radar Range Performance Analysis, D.C.Heath and Co., Lexington.
8. Ament, W.S. (1953). 'Toward a Theory of Reflection by a Rough Surface', Proc. I.R.E., 41(1), p 142.

ANNEX A

Calculation of Detection Threshold
For Fixed Threshold Detectors

```

1201 REM *****
1205 REM UTILITY ROUTINE TO CALC SUM NO=0 TO N-1 OF  $Y_0^M \cdot e^{-Y_0/M}$ 
1206 DEF FN LGT(X)=LOG(X)/LOG(10)
1210 IF N>1 GOTO 1215
1211 Y2=EXP(-Y0)
1212 RATIO=1.0
1213 GOTO 1280
1215 NO=0:ANSWER=0
1216 LIMIT=1.0E35
1217 IF Y0>1 THEN Y1=Y0*10^(37- FN LGT(Y0)):ELSE Y1=1/Y0*10^(37+ FN LGT(Y0))
1220 FACTOR=-LOG(Y1)
1225 REM START OF MAIN LOOP
1230 FACTOR=FACTOR+LOG(Y1)*2
1235 Y1=1/Y1
1240 IF NO=0 THEN Y2=Y1:ELSE Y2=0
1245 REM START OF INNER LOOP
1250 NO=NO+1
1255 Y1=Y0/NO*Y1
1260 Y2=Y2+Y1
1265 IF(NO<(N-1)) AND(Y2<LIMIT) GOTO 1245
1270 ANSWER=ANSWER+EXP(LOG(Y2)+FACTOR-Y0)
1275 IF NO<(N-1) GOTO 1225
1276 IF Y1>0 THEN RATIO=EXP(LOG(ANSWER)+Y0-FACTOR-LOG(Y1))
1278 Y2=ANSWER
1280 RETURN
1290 REM *****
1320 REM START OF MAIN ROUTINE TO CALCULATE THRESHOLD (Y0) FROM N AND PFA
1330 Y0=-1*LOG(PFA)
1335 RATIO=1.0
1340 IF N<=1 THEN 1410
1350 REM First estimate for Y0
1360 Y0=(SQR(-LOG(PFA))+SQR(N)-1)*SQR(-LOG(PFA))+N-SQR(N)
1370 GOSUB 1201
1380 DO=LOG(Y2/PFA)*RATIO
1390 Y0=Y0+DO
1400 IF ABS(DO/Y0)=>3.0E-7 THEN 1370
1410 REM Y0 IS THRESHOLD FOR FIXED THRESHOLD DETECTOR
1420 RETURN
1425 REM *****

```

ANNEX B

Calculation of Pd for Marcum, Swerling and Weinstock Targets

```

1425 REM *****
1430 REM CALCULATE Pd FROM S/N (X dB), CHI-SQUARE PARAMETER (K), N AND Y0
1440 ELIMIT=1/(10*N):Y2=PFA
1443 Y1=PFA/RATIO
1444 NO=N
1450 X=10^(X/10)
1460 S1=Y2
1470 X1=(K/(K+N*X))^K
1480 X2=X1
1490 X3=X*N/(K+N*X)
1500 D1=K-1
1510 M=1
1520 R1=0
1525 IF X2=0 THEN GOSUB 1661
1526 REM RESUME AFTER UNDERFLOW LIMIT REACHED
1530 L1=R1
1540 Y1=Y1/NO*Y0
1550 Y2=Y2+Y1
1560 S1=S1+Y1*(1-X2)
1570 E1=(1-X2)*(1-Y2)
1580 R1=S1+E1
1590 X1=(D1+M)/M*X1*X3
1600 X2=X2+X1
1605 IF(X2>1) THEN X2=1
1610 M=M+1
1620 NO=NO+1
1630 IF ABS(1-L1/R1)=>3.0E-7 THEN 1530
1640 IF E1=>ELIMIT THEN 1530
1650 REM R1 IS THE PROBABILITY OF DETECTION
1655 RETURN
1656 REM *****
1660 REM SUBROUTINE TO SCALE FOR UNDERFLOW
1661 X4=0:X5=K*(LOG(K)-LOG(K+N*X))
1662 X6=LOG(X3)
1663 REM JUMP HERE TILL LIMIT
1664 Y1=Y1/NO*Y0
1665 Y2=Y2+Y1
1666 S1=S1+Y1
1667 X4=X4+X6+LOG(D1+M)-LOG(M)
1668 X1=EXP(X5+X4)
1669 X2=X2+X1
1670 M=M+1
1671 NO=NO+1
1672 IF X2=0 THEN GOTO 1663
1673 RETURN
1675 REM *****

```

ANNEX C

Calculation of Required Signal-to-Noise (Do)

```

8000 REM *****
8001 REM routine to solve roots of f(x)=R1 by secant method
8002 REM SNdBn IS CURRENT ESTIMATE IN dB OF S/N REQUIRED FOR Pd = PROB
8003 DEF FN LGT(X)=LOG(X)/LOG(10)
8004 LN= FN LGT(N)
8005 REM
8006 PROB=0.95
8007 PROBLIMIT=0.00001
8008 REM ITERATION WILL BE STOPPED WHEN SNdB3 = PROB +/- PROBLIMIT
8010 REM FIRST ESTIMATE OF REQUIRED S/N IS FIT OF SOLUTIONS FOR PD=0.33
8011 IF N<3 THEN SNdB3=10.5924-8.74904*LN
8012 IF N>=3 THEN SNdB3=7.138+1.018/LN-5.353*LN
8013 SNdB3=SNdB3+4.343* FN LGT(PFA/1.0E-6)/ FN LGT(PFA)
8014 REM SECANT METHOD SEEDED WITH 2 POINTS STRADDLING Pd=0.33
8015 SNdB1=SNdB3-1.0:X=SNdB1:GOSUB 1430:PROB1=R1
8020 SNdB2=SNdB3+1.0:X=SNdB2:GOSUB 1430:PROB2=R1
8025 REM
8028 IF (PROB2=0) AND (PROB1=0) THEN SNdB3=SNdB3+0.25:GOTO 8015
8029 IF (PROB2=1) AND (PROB1=1) THEN SNdB3=SNdB3-0.25:GOTO 8015
8030 SLOPE=(SNdB2-SNdB1)/(PROB2-PROB1)
8035 TESTSLOPE=(PROB-PROB2)*SLOPE
8036 IF TESTSLOPE>3 THEN SNdB3=SNdB2+ FN LGT(TESTSLOPE):GOTO 8050
8037 IF TESTSLOPE<-3 THEN SNdB3=SNdB2- FN LGT(-TESTSLOPE):GOTO 8050
8040 SNdB3=SNdB2+TESTSLOPE
8050 X=SNdB3:GOSUB 1430:PROB3=R1
8055 REM SNdB3 IS CURRENT ESTIMATE OF Do FOR Pd=100*PROB3 %
8060 IF ABS(PROB3-PROB)<PROBLIMIT THEN GOTO 8100
8070 SNdB1=SNdB2:PROB1=PROB2
8080 SNdB2=SNdB3:PROB2=PROB3
8090 GOTO 8030
8100 PRINT "ITERATION STOPPED AT ";SNdB3;" dB = ";100*PROB3;" %"
8110 RETURN
9000 REM *****

```


ANNEX D

Calculation of Paint Probability for Non-fluctuating Targets

```

1425 REM *****
1430 REM **** PROBABILTY OF DETECTION FOR NON-FLUCTUATING TARGETS***
1431 REM CALCUATION OF Pd AT : Signal-to-Noise = X dB
1432 REM          Probability of False Alarm = PFA
1433 REM          N Pulses Non-coherently Integrated
1444 REM          Fixed Threshold = Y0
1445 REM
1440 Y2=PFA
1443 Y1=PFA/RATIO
1444 NO=N
1450 X=10^(X/10)
1460 S1=Y2
1465 X3=N*X
1470 X1=EXP(-X3)
1480 X2=X1
1492 X6=LOG(X3)
1510 M=1
1520 R1=0
1525 REM TEST FOR UNDERFLOW CONDITION
1526 IF X2=0 THEN GOSUB 1661
1530 L1=R1
1540 Y1=Y1/NO*Y0
1550 Y2=Y2+Y1
1560 S1=S1+Y1*(1-X2)
1570 E1=(1-X2)*(1-Y2)
1580 R1=S1+E1
1590 X1=X3/M*X1
1600 X2=X2+X1
1610 M=M+1
1620 NO=NO+1
1630 IF ABS(1-L1/R1)>3.0E-7 THEN 1530
1640 IF E1>0.001 THEN 1530
1650 REM R1 IS THE PROBABILITY OF DETECTION
1655 RETURN
1656 REM *****
1660 REM USE SCALING ROUTINE WHILE UNDERFLOW CONDITION EXISTS
1661 X4=0
1662 X6=LOG(X3)
1663 REM JUMP HER TILL LIMT
1664 Y1=Y1/NO*Y0
1665 Y2=Y2+Y1
1666 S1=S1+Y1
1667 X4=X4+X6-LOG(M)
1668 X1=EXP(X4-X3)
1669 X2=X2+X1
1670 M=M+1
1671 NO=NO+1
1672 IF X2=0 THEN GOTO 1663
1673 RETURN
1674 REM *****

```

ANNEX E

Main Program for Contour
VCD calculations.

```

1  REM DEFINE FUNCTIONS REQUIRED FOR GEOMETRY ROUTINES
6  DEF FN LGT(X)=0.43429448*LOG(X)
7  DEF FN ASN(X)=ATN(X/SQR(1-X^2))
8  DEF FN SL(X)=SQR((HH2-HH1)^2+4*(A1+HH1)*(A1+HH2)*(SIN(X/(2*A1))))^2)
9  DEF FN GR(X)=2*A1* FN ASN(SQR(((X^2-(HH2-HH1)^2)/(4*(A1+HH1)*(A1+HH2))))
12 DEF FN EL(X)= FN ASN((2*A1*(HH2-HH1)+HH2^2-HH1^2-X^2)/(2*(A1+HH1)*X))
13 DEF FN IND(X)= FN ASN((2*A1*HH1+HH1^2+X^2)/(2*(A1+HH1)*X))
2190 REM VCD ALGORITHM IS ITERATIVE OR R^4 SCALING ( I OR S )
2196 REM 30 MULTIPATH LOBES CALCULATED USING DEFAULT PARAMETERS (POINTS%=300)
2199 REM *****
2200 REM START OF MAIN PROGRAM
2201 R7=SQR(2*A1/M1)*(SQR(H1))
2202 MINELEV=-1.0* FN ASN(H1M/R7+R7/2/A1):MAXELEV=TILT+1.1*B1
2203 PRINT"MIN ELEVATION = ";57.3*MINELEV;" DEGREES"
2204 DBLIMIT=0.25:REM 0.25 dB RESOLUTION FOR ITERATIVE ALGORITHM
2205 PRINT"CALCS CARRIED OUT TO ";57.3*MAXELEV;" DEGREES"
2206 INCELEV=0.1* FN ASN(W/(2*H1))
2207 ELTHETA(1)=0.70*MINELEV
2208 PRINT"USING LOOKUP TABLE PROVIDED,WHAT IS THE SIGNAL-TO-NOISE RATIO"
2209 PRINT"REQUIRED FOR THIS RADAR'S VCD CONTOUR":INPUT THRESH
2210 LINP1=10^(P1/10)
2211 QTHRESH=10^(-THRESH/40):R0=R0*QTHRESH
2212 FOR I=1 TO POINTS%
2213   FIRSTSLANT=ABS(R0*F1*(1+R1*F2/F1))
2214   IF I=1 THEN GOTO 2220
2215   ELTHETA(I)=ELTHETA(I-1)+INCELEV
2216   IF ELTHETA(I)>MAXELEV THEN I=POINTS% :GOTO 2400
2220   THETA=ELTHETA(I):GOSUB 920
2225   REM First estimate of range
2227   SLANT=FIRSTSLANT
2240   PRINT" FIRST SLANT = ";SLANT
2242   LOWLIMIT=10
2245   ITERATION=0
2250   REM ark** Compute first estimate of altitude
2251   IF ALG$="I" GOTO 2255
2252   IF ITERATION=2 GOTO 2375
2255   HH1=H1M
2257   H9(I)=SLANT^2+2*SLANT*(A1+HH1)*SIN(ELTHETA(I))+(A1+HH1)^2
2258   H9(I)=M1*(SQR(H9(I))-A1)
2260   PRINT"HEIGHT = ";H9(I);" FEET"
2261   HH1=H1M:HH2=H9(I)/M1:G(I)= FN GR(SLANT)
2262   H2=H9(I)
2263   G8=G(I)
2265   ITERATION=ITERATION+1
2270   R7=SQR(2*A1/M1)*(SQR(H1)+SQR(H9(I)))
2280   REM Compute target multipath geometry
2290   GOSUB 2680
2300   REM Compute clutter return for ith point - C7(I)
2310   GOSUB 3400
2320   REM Calculation/interpolation of pattern propagation factor - F(I)
2330   GOSUB 2470
2340   REM radar equation
2350   F(I)=K6+F(I)+RCS-40* FN LGT(SLANT)-2*L3*SLANT

```

Main program (cont'd)

```

2352 NOISE=10* FN LGT(LINP1+(10^(C7(I)/10)))
2353 INCSLANT=SLANT-OLDSLANT
2354 OLDEXCESS=EXCESS:OLDSLANT=SLANT
2355 EXCESS=F(I)-NOISE:IF ABS(EXCESS-THRESH)<DBLIMIT THEN GOTO 2375
2356 INCXCESS=EXCESS-OLDEXCESS
2357 IF(ABS(EXCESS-THRESH)>ABS(LOWLIMIT)) THEN GOTO 2359
2358 LOWLIMIT=EXCESS-THRESH:LOWG=G(I):LOWR=OLDSLANT:LOWH=H9(I):LOWP=F(I)
2359 IF ITERATION<10 THEN GOTO 2365
2360 EXCESS=LOWLIMIT+THRESH:G(I)=LOWG:OLDSLANT=LOWP:H9(I)=LOWH:F(I)=LOWP
2361 GOTO 2375:REM END ITERATION AND USE SMALLEST EXCESS IN VCD
2362 IF ITERATION<2 THEN SLANT=SLANT*QTHRESH*(10^(EXCESS/40))
2363 IF ITERATION<2 THEN GOTO 2369
2365 IF ITERATION<4 THEN SLANT=SLANT*(QTHRESH*(10^(EXCESS/40)))^0.5
2366 IF ITERATION<4 THEN GOTO 2369
2367 SLANT=SLANT+(THRESH-EXCESS)*INCSLANT/INCXCESS
2368 IF SLANT<0 THEN SLANT=2*R0*RND(1)+0.0811*W5
2369 PRINT"SLANT= ";OLDSLANT;" ELEV= ";57.3*ELTHETA(I);" EXCESS= ";EXCESS;
2370 PRINT:GOTO 2250
2375 RSLANT(I)=OLDSLANT
2380 REM Printout
2390 GOSUB 2840
2395 IMAX=I
2400 NEXT I
2450 REM *****

```

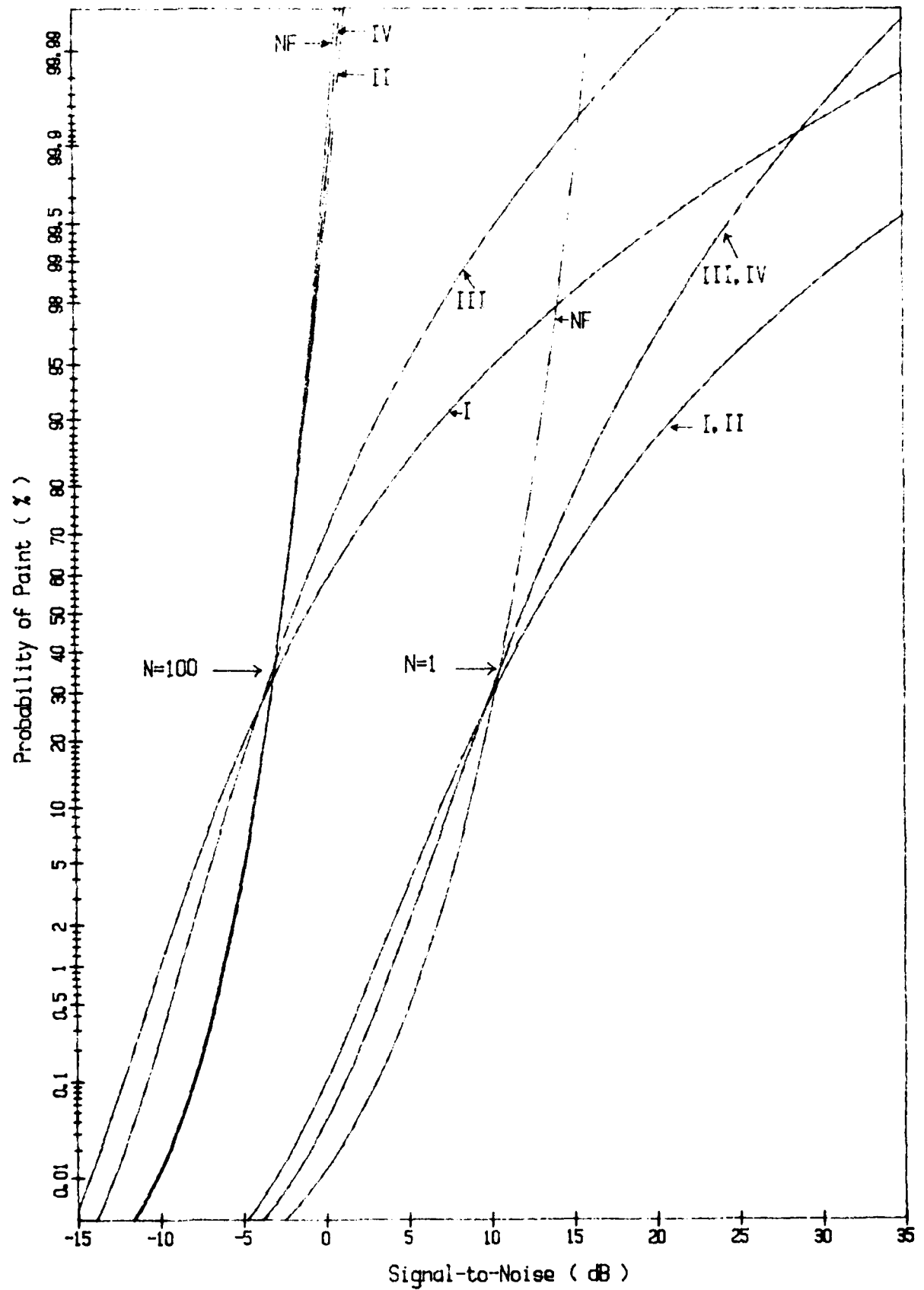


Figure 1. Probability of paint for Swerling case I - IV and non-fluctuating targets. $PFA=0.000001$, $N=1$ and $N=100$.

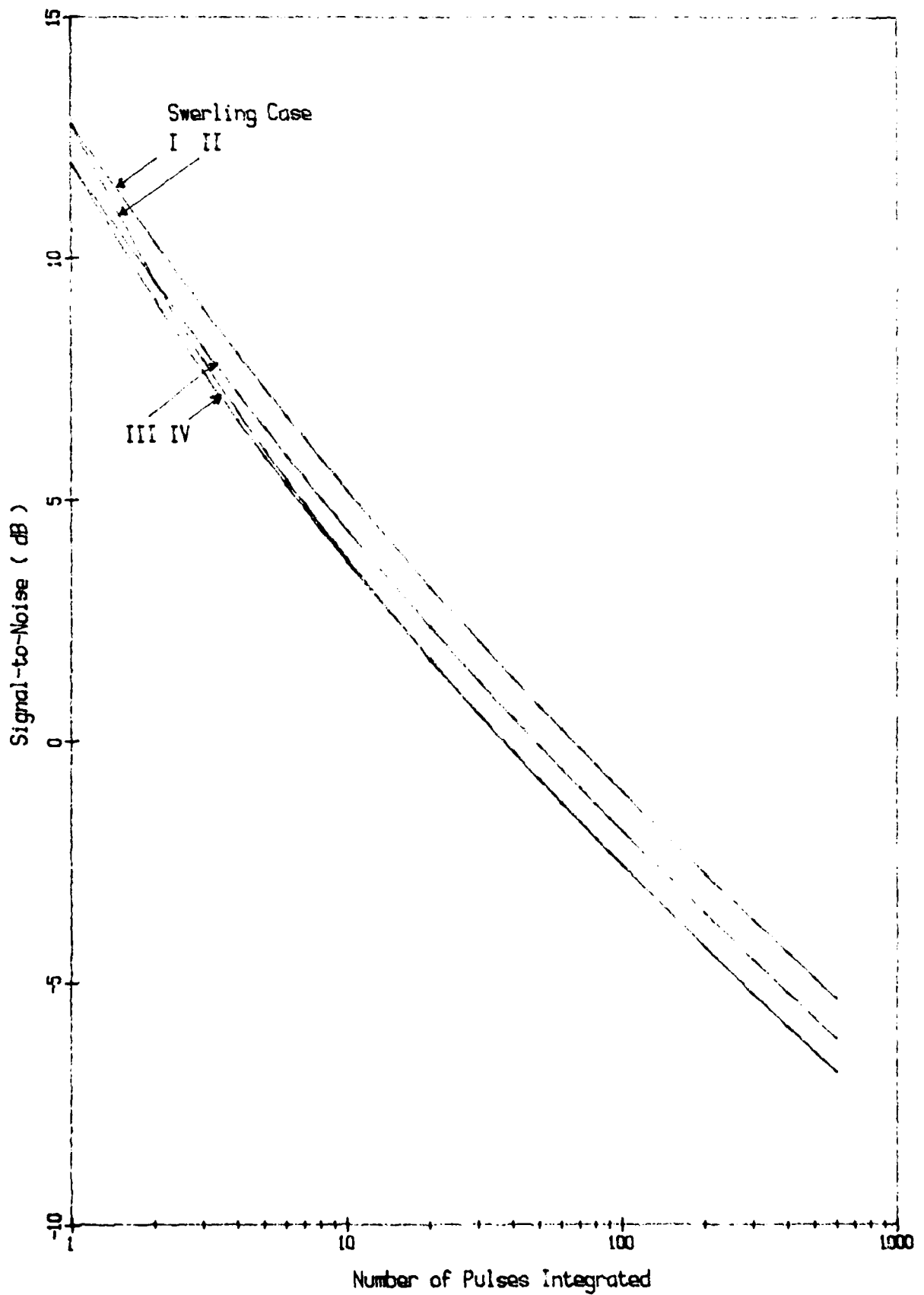


Figure 2. Signal-to-noise required for 50% point probability.
PFA = 0.000001, Swerling case I-IV targets.

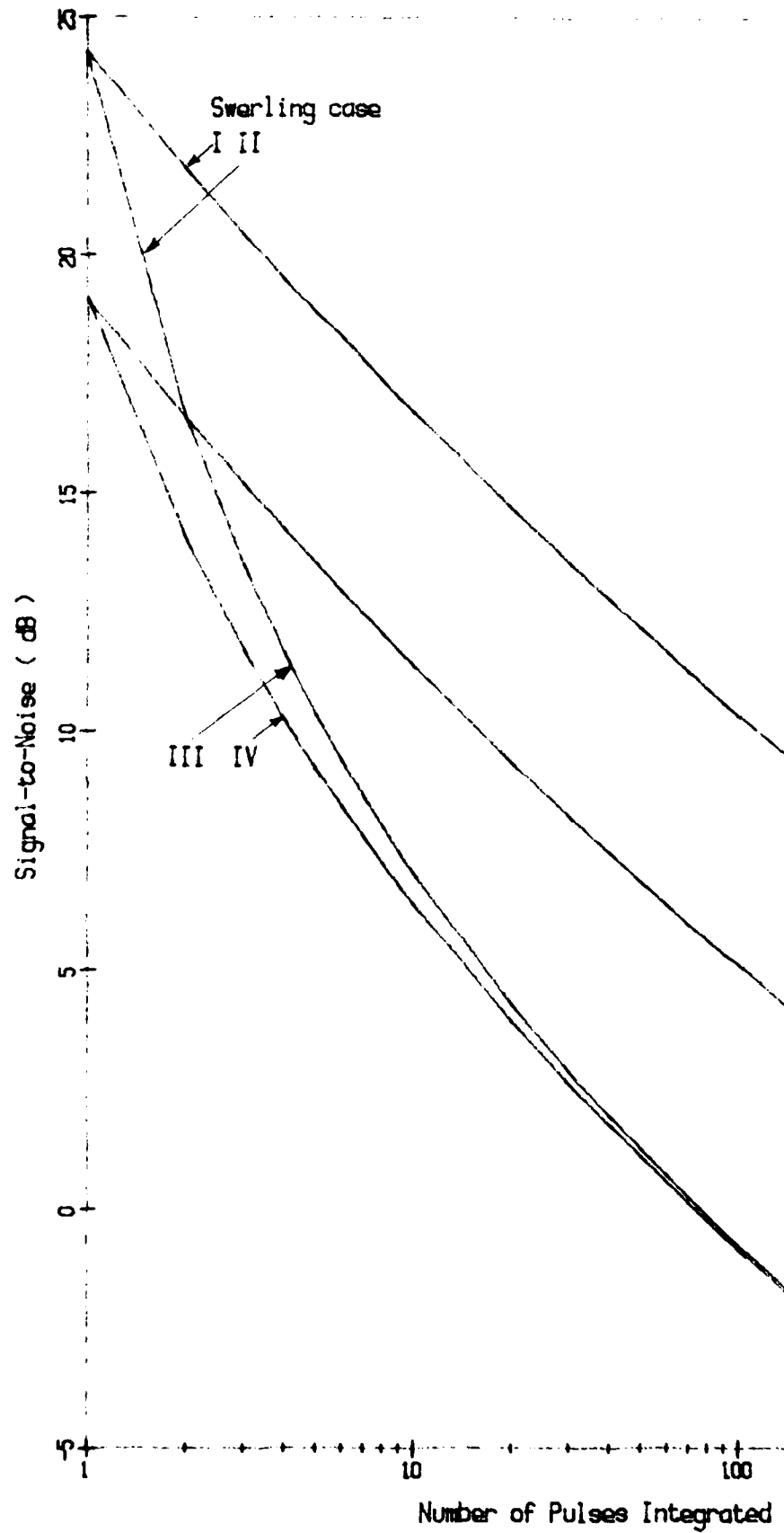


Figure 3. Signal-to-noise required for 95% point probx
 $PFA = 0.000001$, Swerling case I-IV targets.

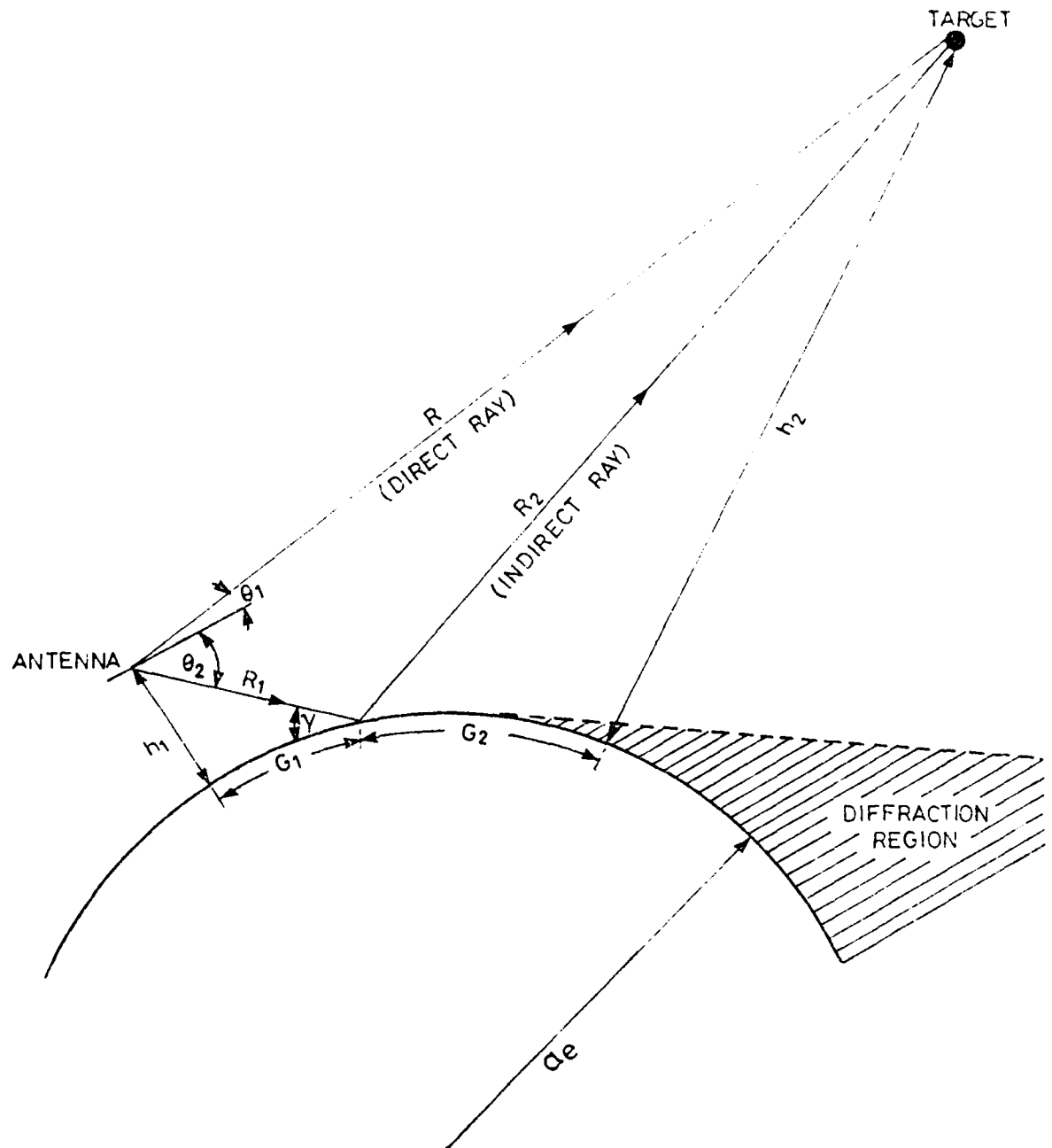


Figure 4. Multipath geometry with symbols as used in text.

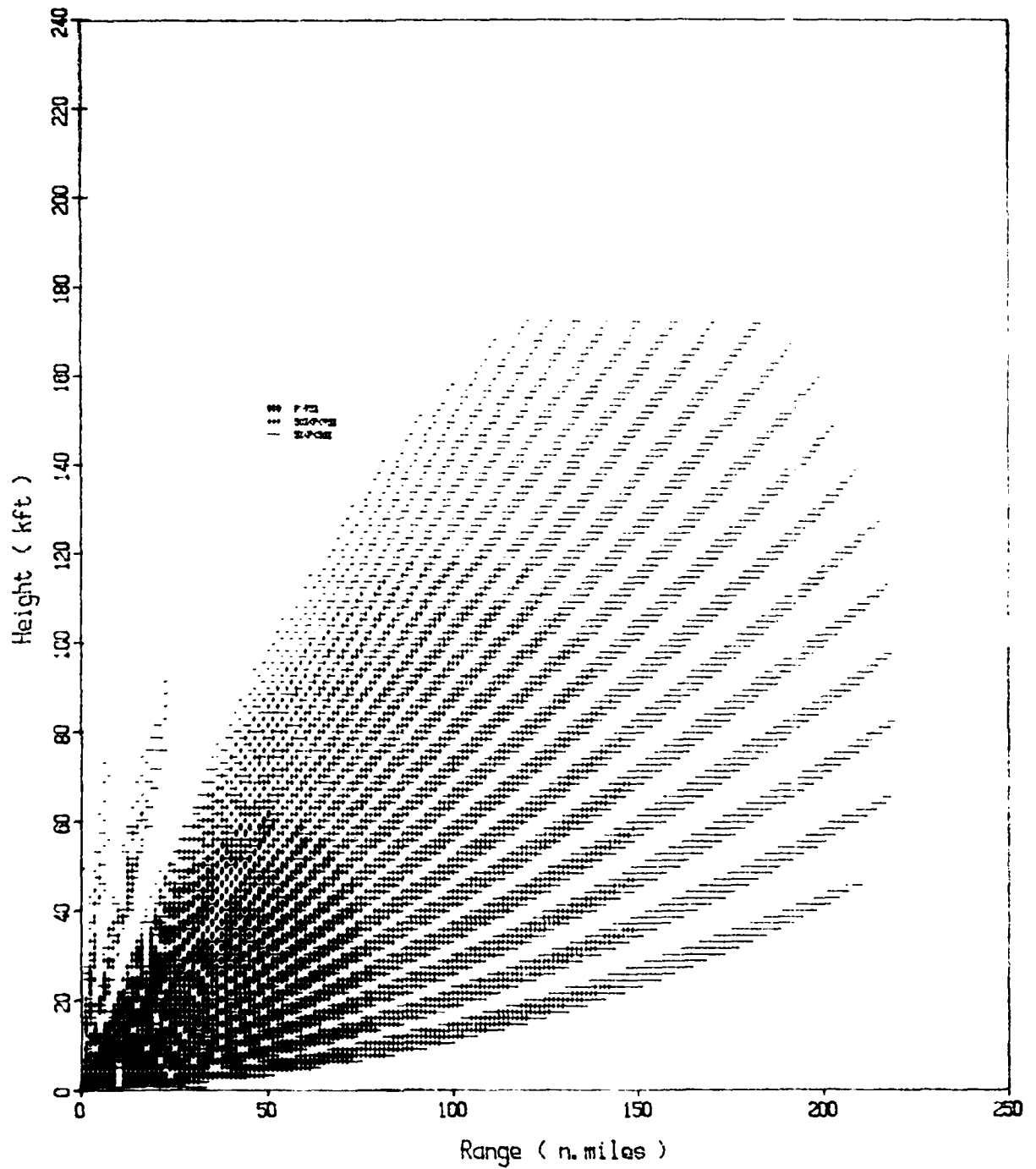


Figure 5. Vertical coverage diagram for UHF radar.

Sea state : 0

Number of pulses integrated : 75

Target : 1 m^2 , Swerling case I

Grey scales : 4

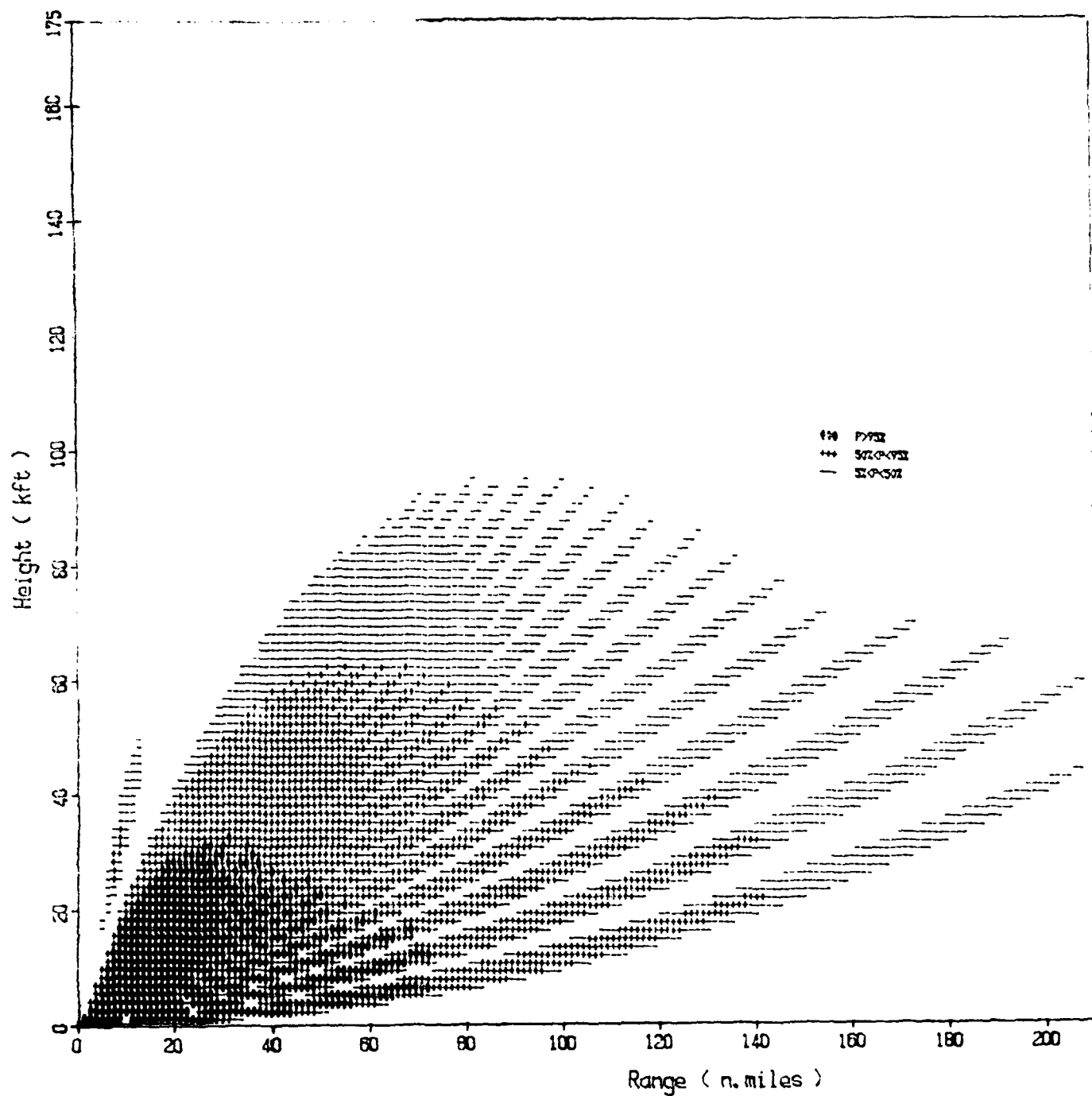


Figure 6. Vertical coverage diagram for UHF radar.

Sea state : 6

Number of pulses integrated : 75

Target : 1 m^2 , Swerling case I

Grey scales : 4

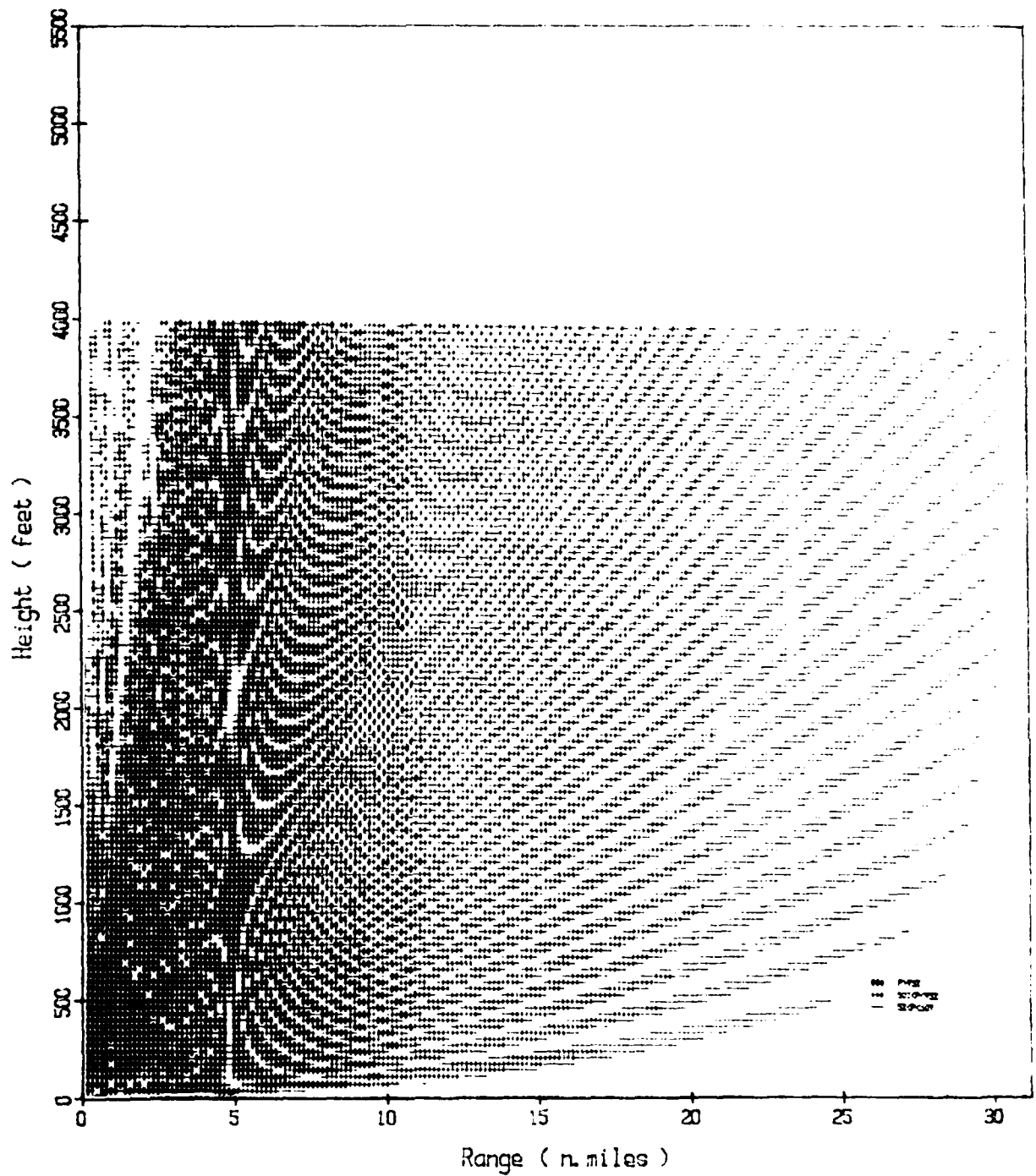


Figure 7. Vertical coverage diagram for G-band radar.

Sea state : 0

Number of pulses integrated : 5

Target : 1 m^2 , Swerling case I

Grey scales : 4

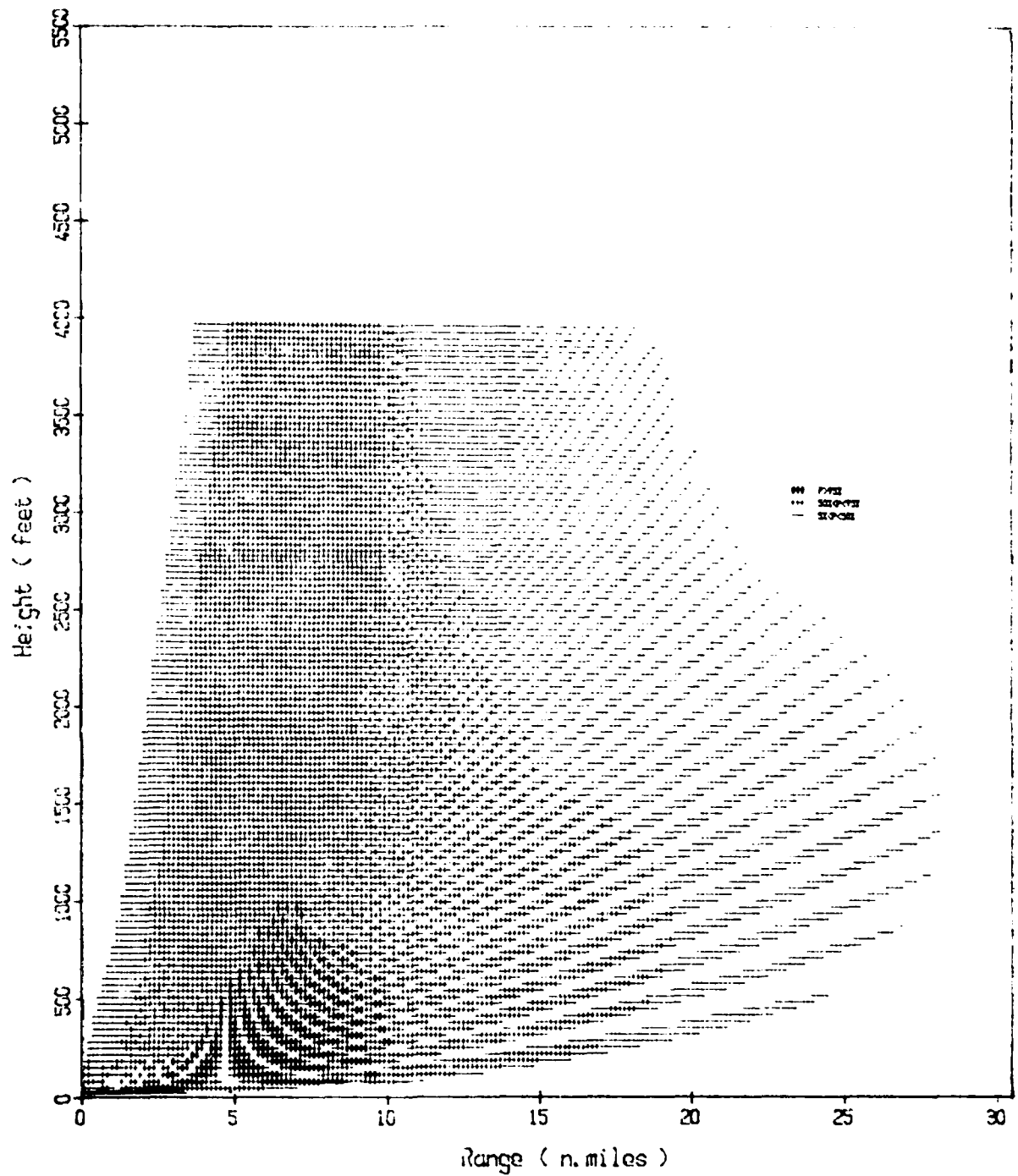


Figure 8. Vertical coverage diagram for G-band radar.
 Sea state : 3
 Number of pulses integrated : 5
 Target : 1 m^2 , Swerling case 1
 Gray scales : 4

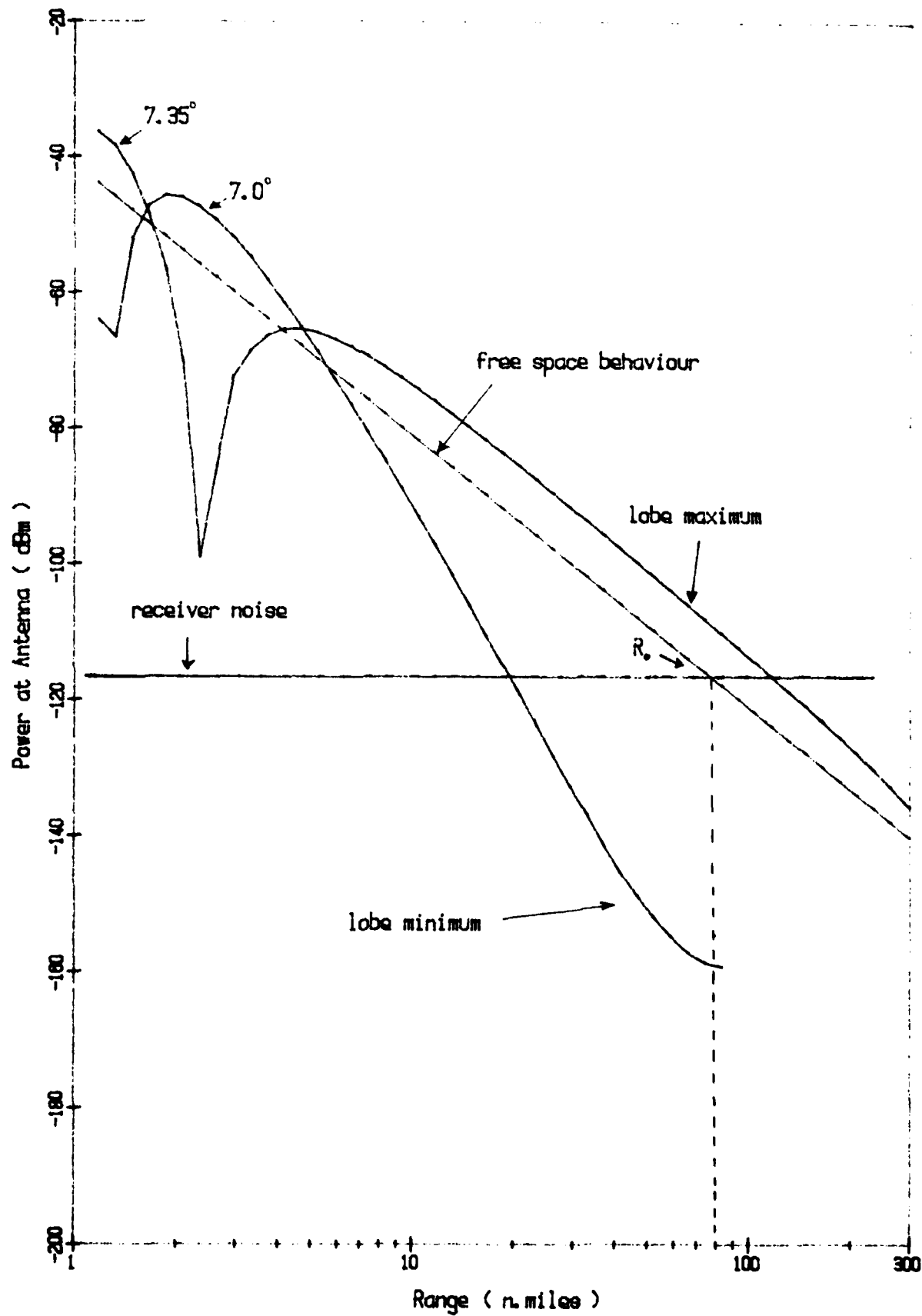


Figure 9. Signal returns for UHF radar at constant elevation angle of 7.0 and 7.35 degrees. Sea state 0.

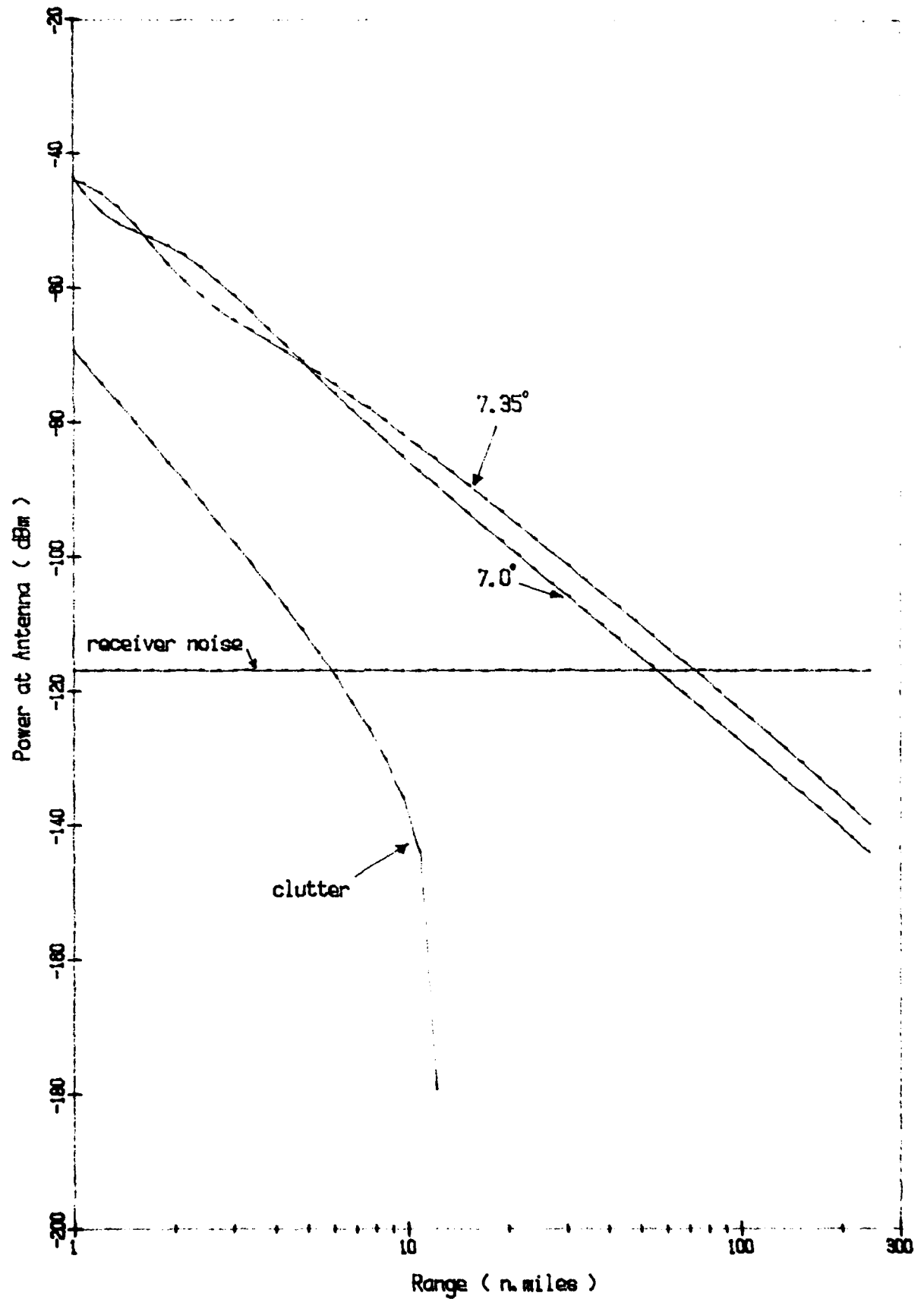


Figure 10. Signal returns for UHF radar at constant elevation angle of 7.0 and 7.35 degrees. Sea state 6.

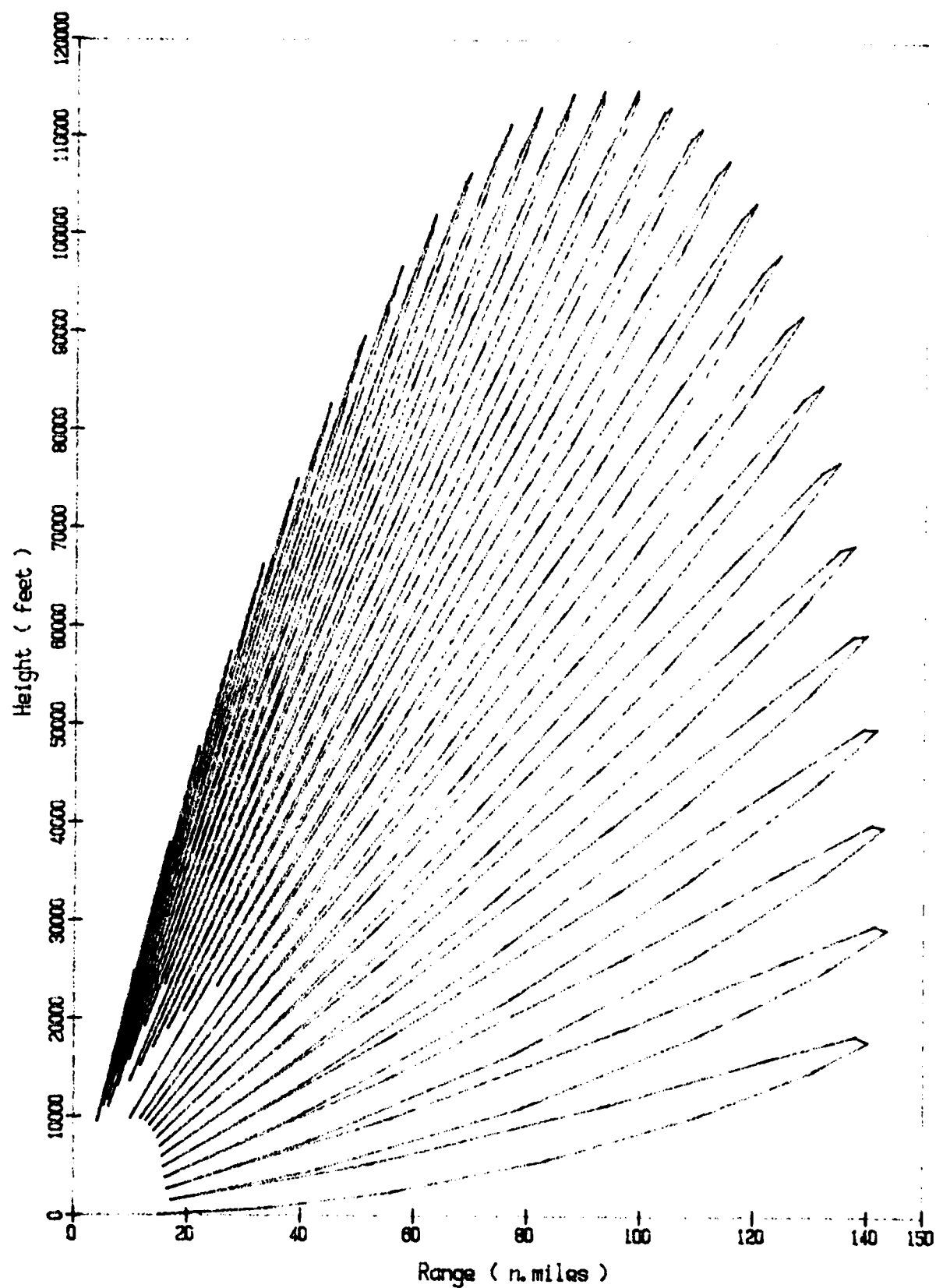


Figure 11. Contour VCD for UHF radar.

Sea state : 0

Signal-to-noise : 0 dB (± 0.25)

Algorithm : Iterative

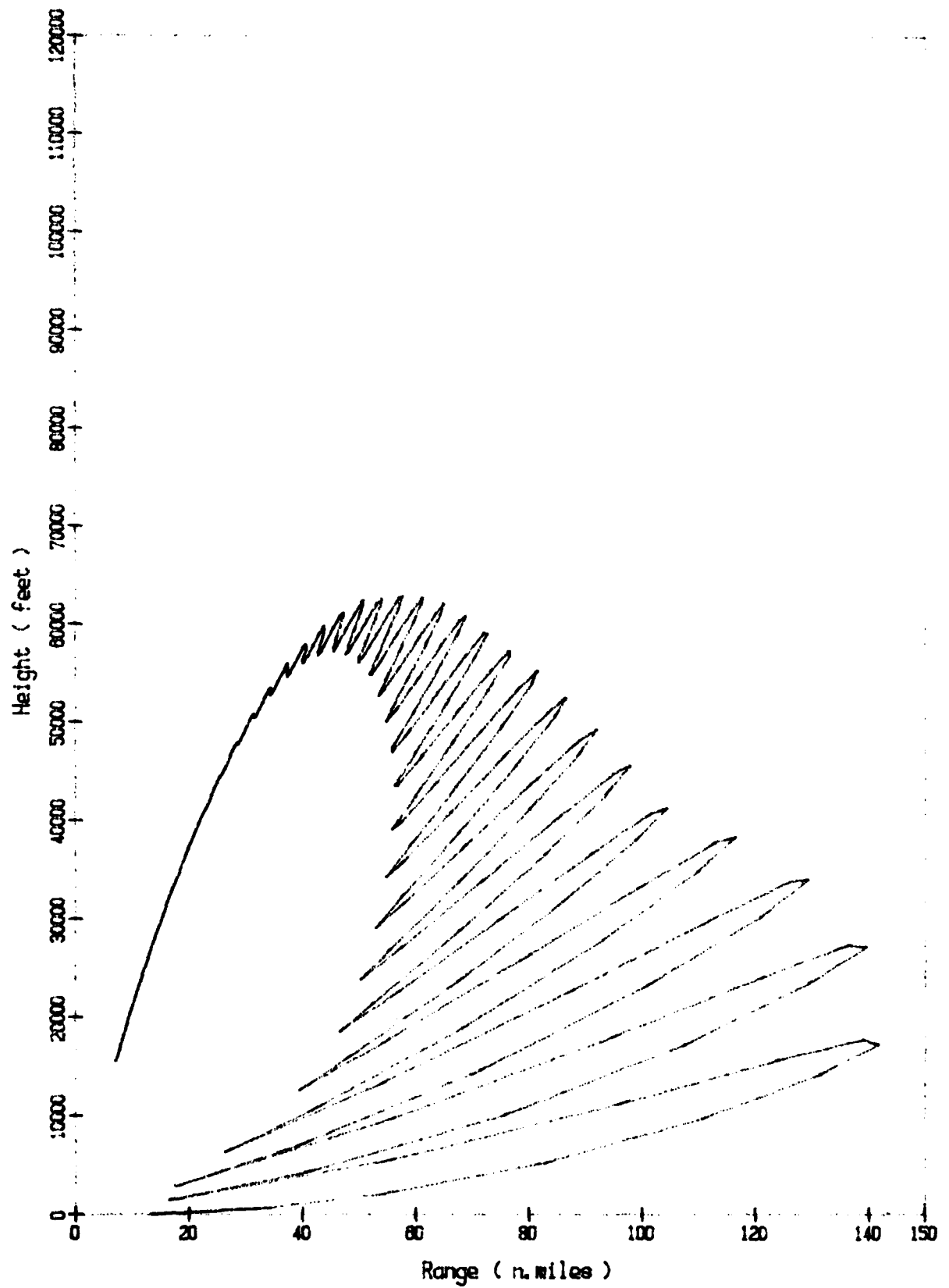


Figure 12. Contour VCD for UHF radar.

Sea state : 8

Signal-to-noise : 0 dB (± 0.25)

Algorithm : Iterative

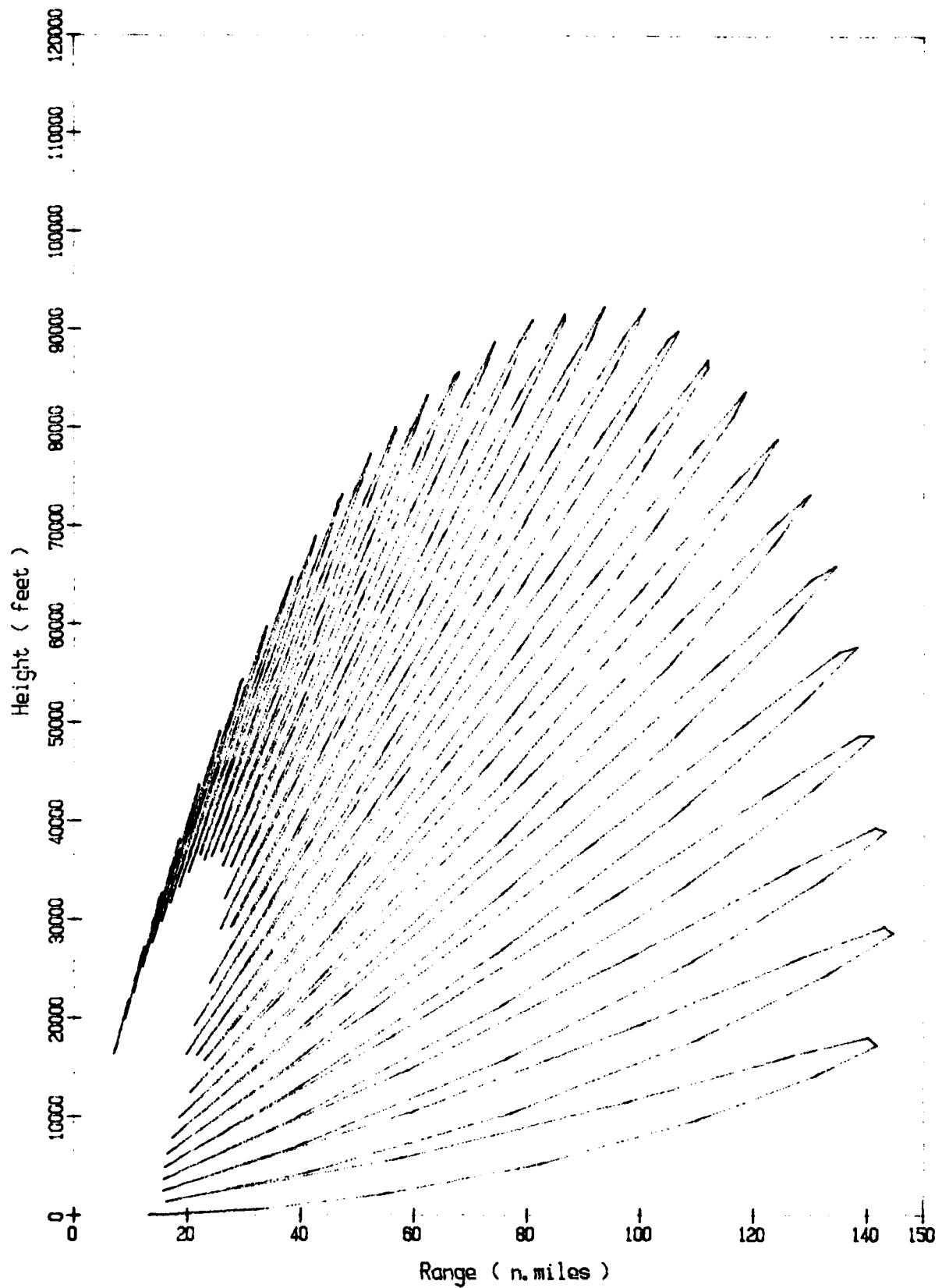


Figure 13. Contour VCD for UHF radar.

Sea state : 3

Signal-to-noise : 0 dB (± 0.25)

Algorithm : Iterative

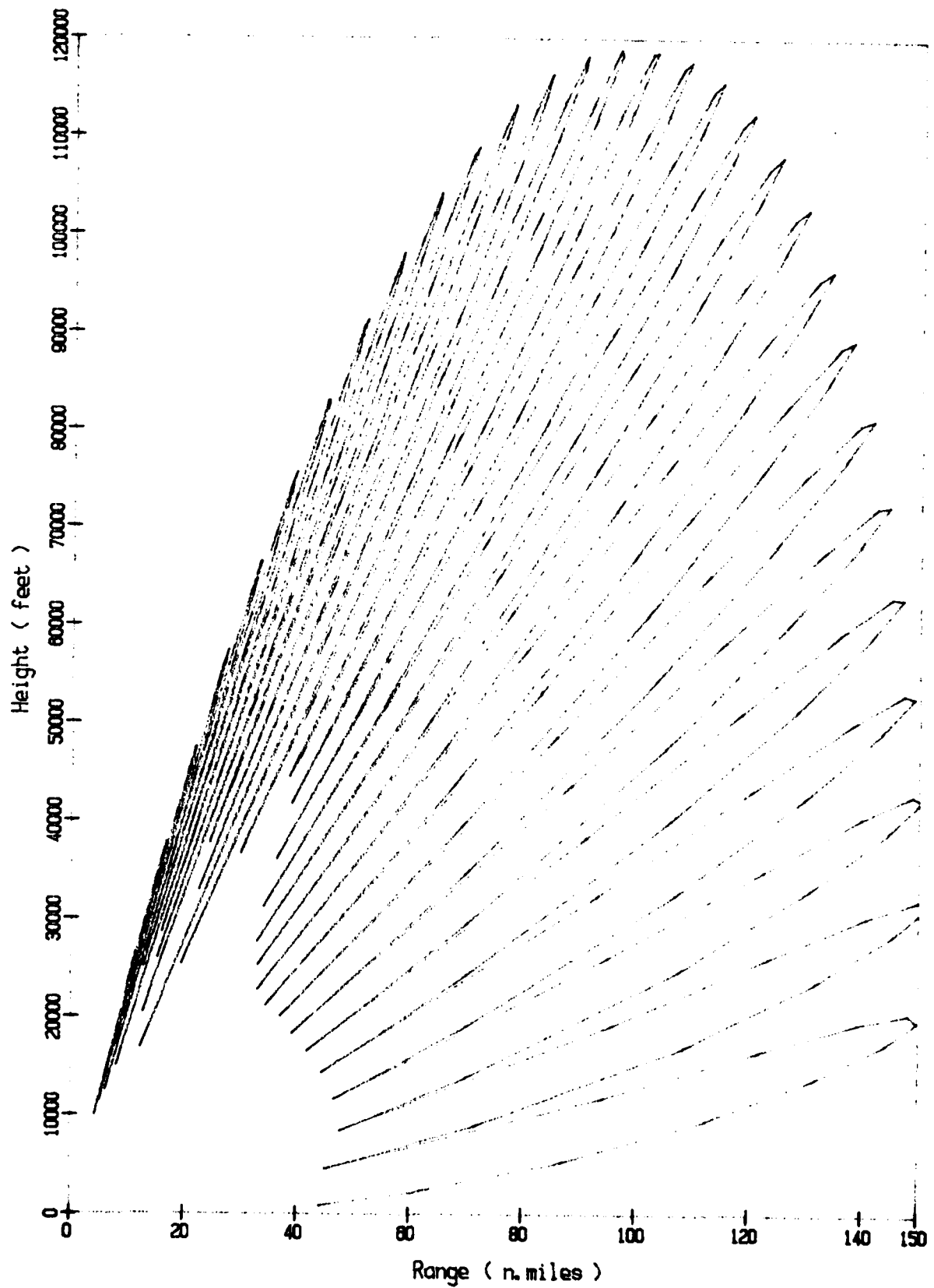


Figure 14. Contour VCD for UHF radar.
Sea state : 0
Signal-to-noise : 0 dB
Algorithm : Scaling

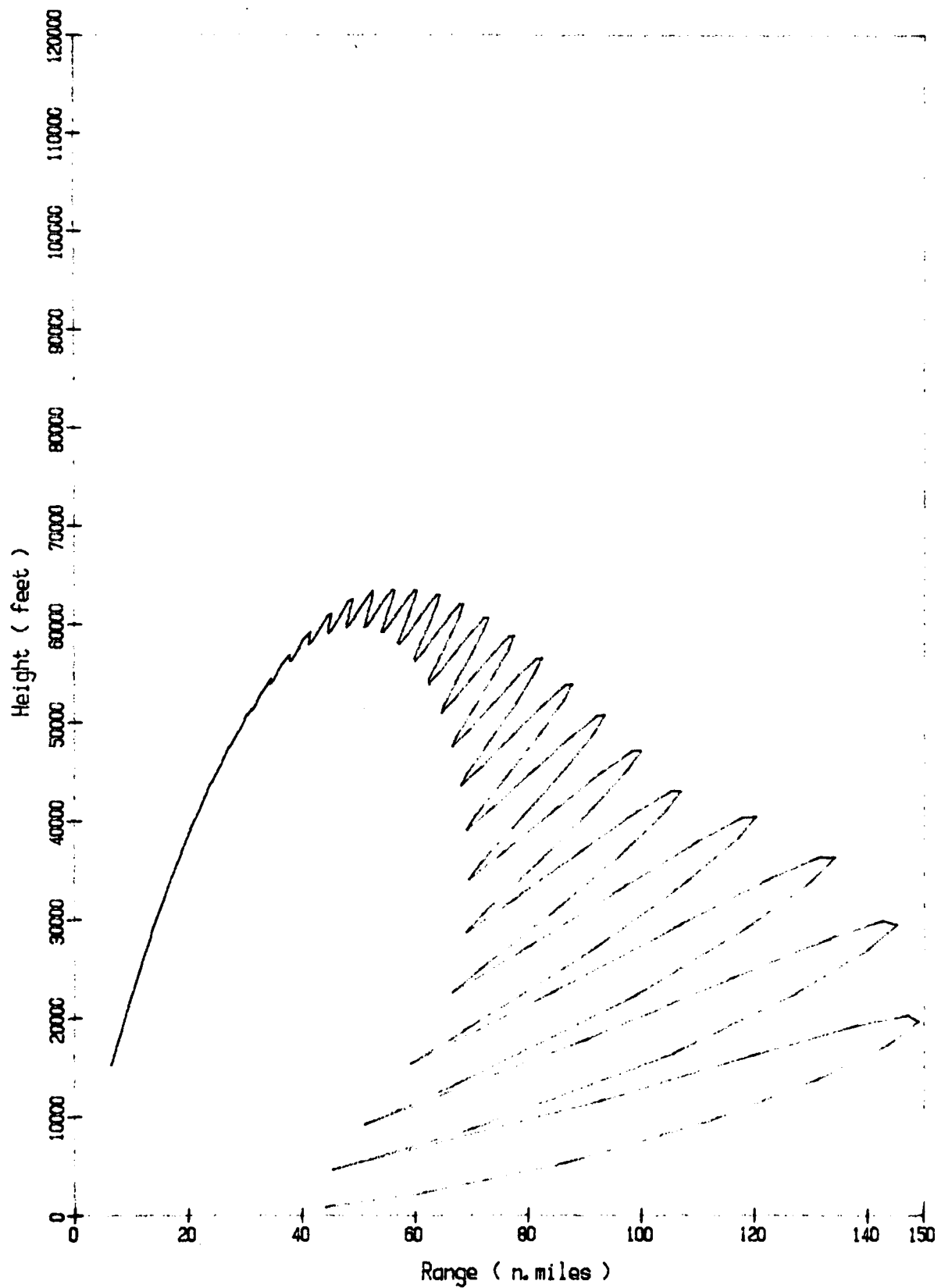


Figure 15. Contour VCD for UHF radar.

Sea state : 6

Signal-to-noise : 0 dB

Algorithm : Scaling

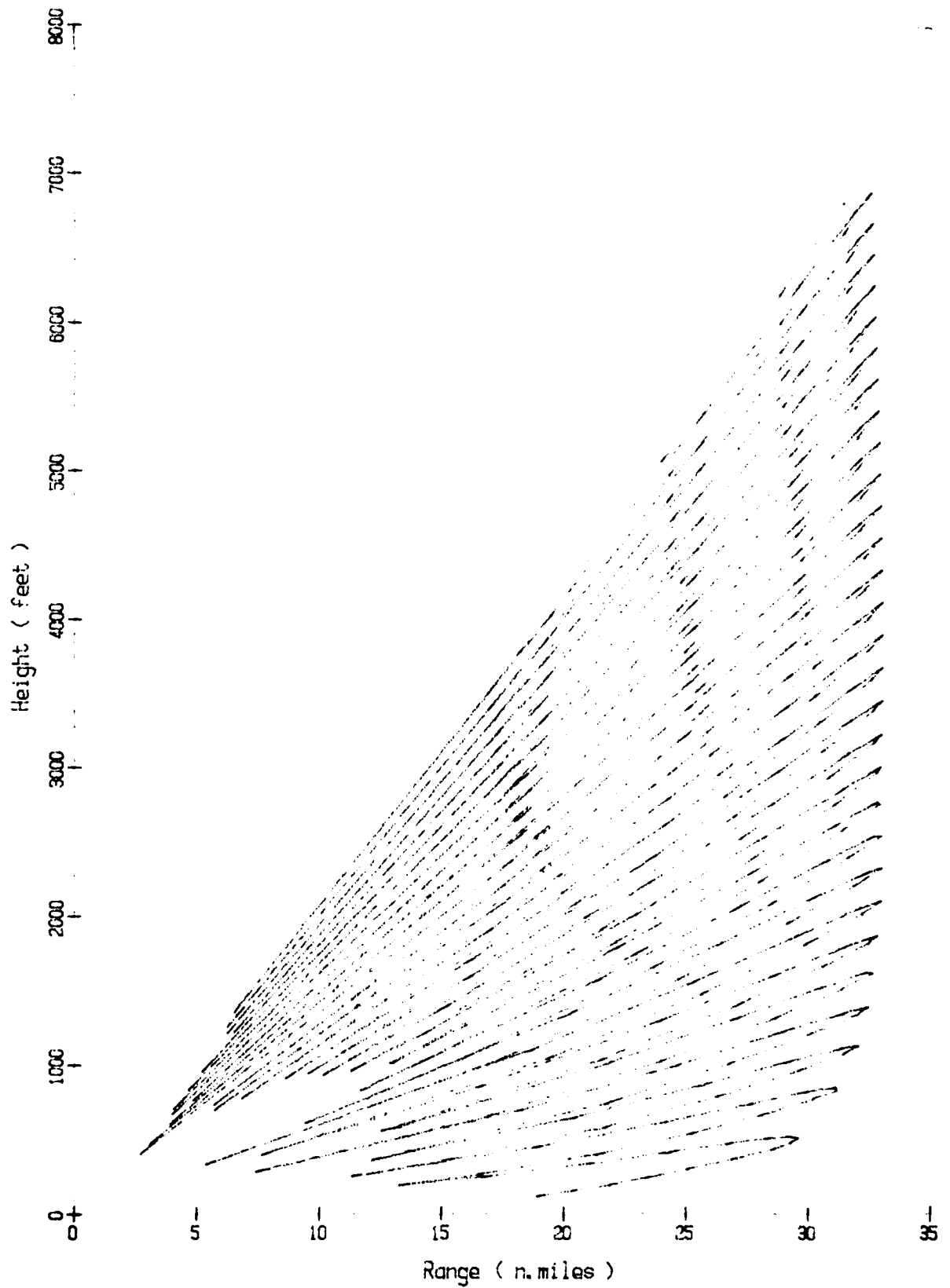


Figure 16. Contour VCD for G-band radar (low angle coverage only).

Sea state : 0

Signal-to-noise : 0 dB

Algorithm : Scaling

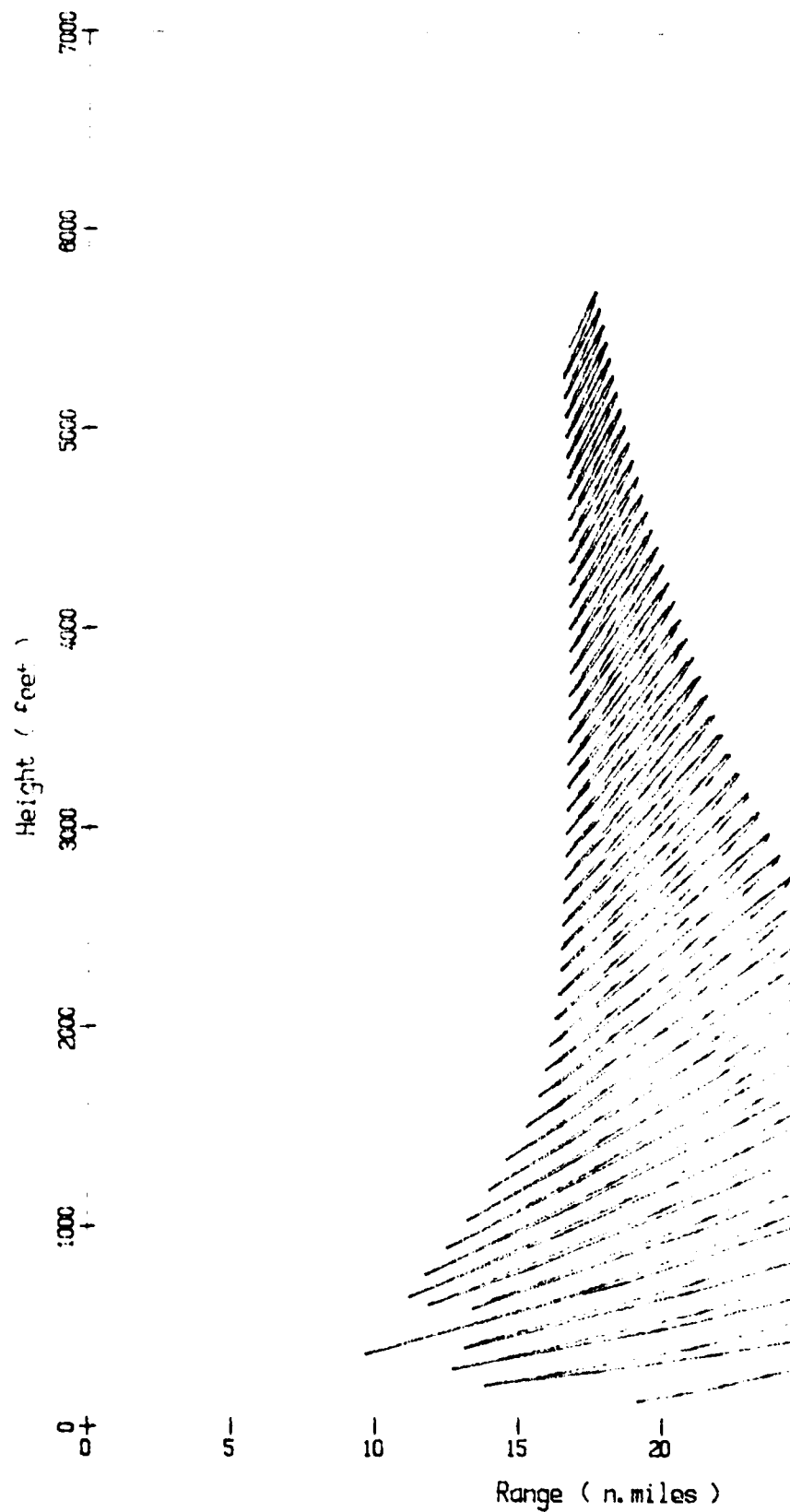


Figure 17. Contour VCD for G-band radar (low angle α)
Sea state : 3
Signal-to-noise : 0 dB
Algorithm : Scaling

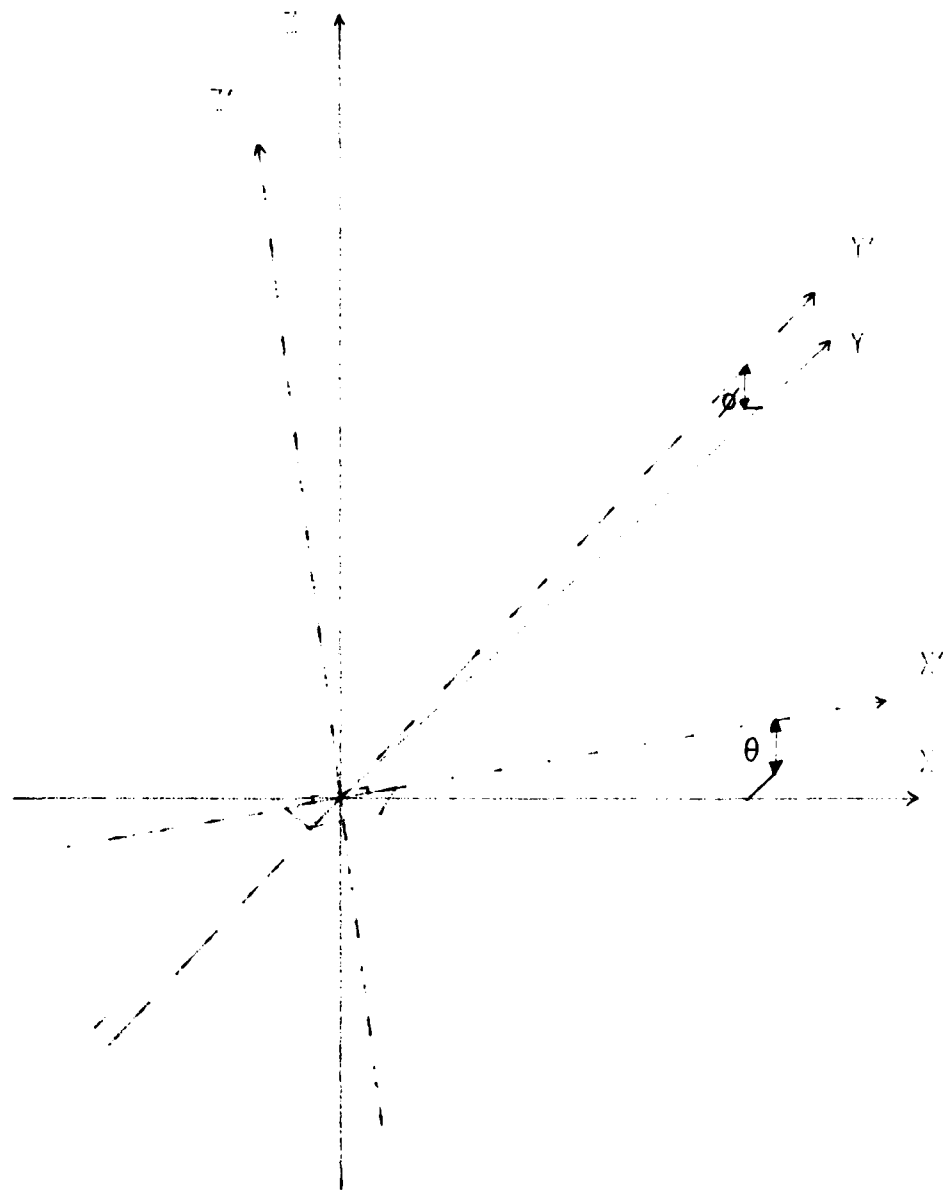


Figure 18. Reference axis systems for discussion of ship motion.

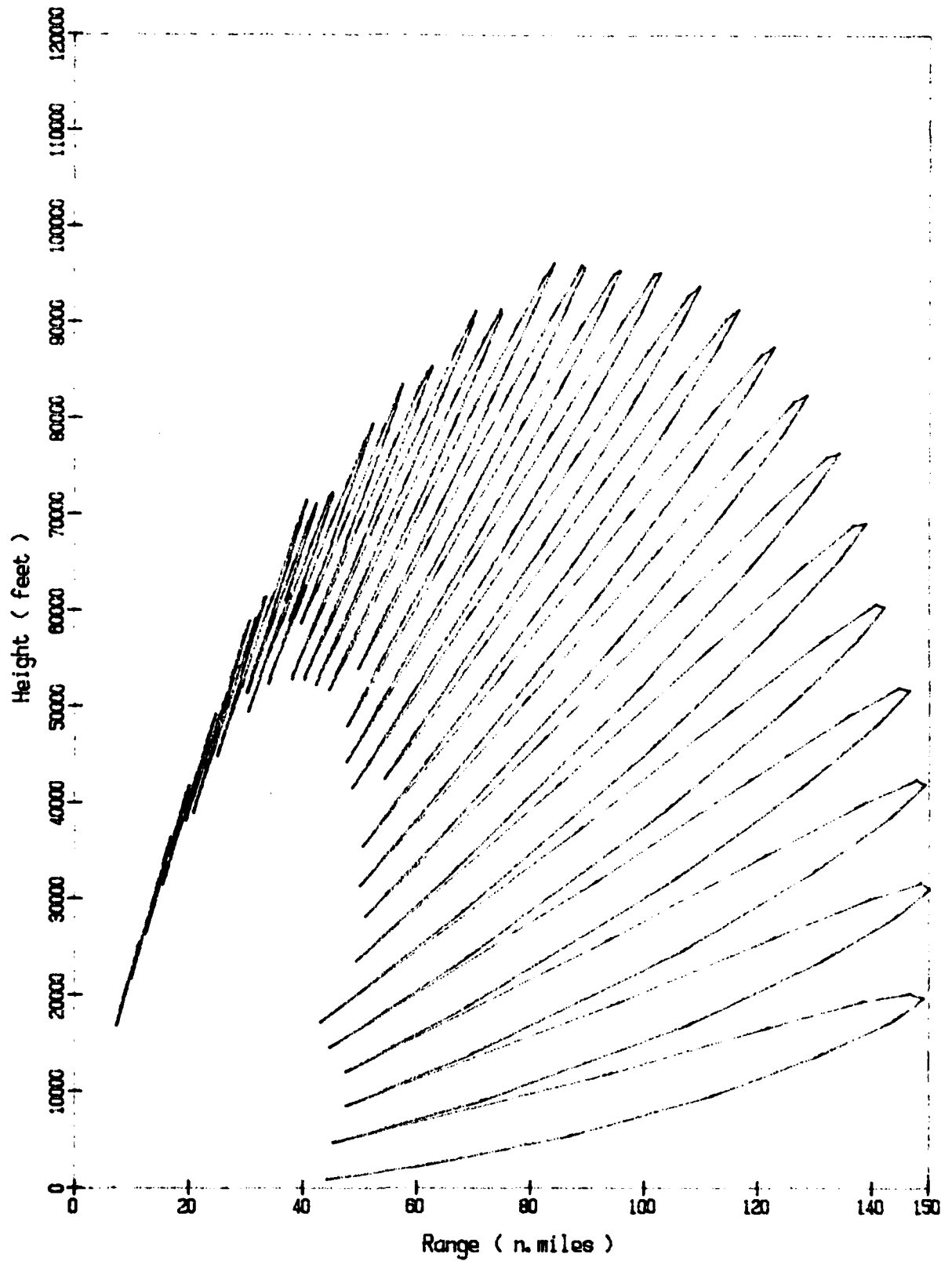


Figure 19. Simulation of the effect of varying antenna tilt for UHF radar
Sea state : 3
Signal-to-noise : 0 dB
Antenna tilt : Random between -10% and + 10% of vert beamwidth
Algorithm : Scaling

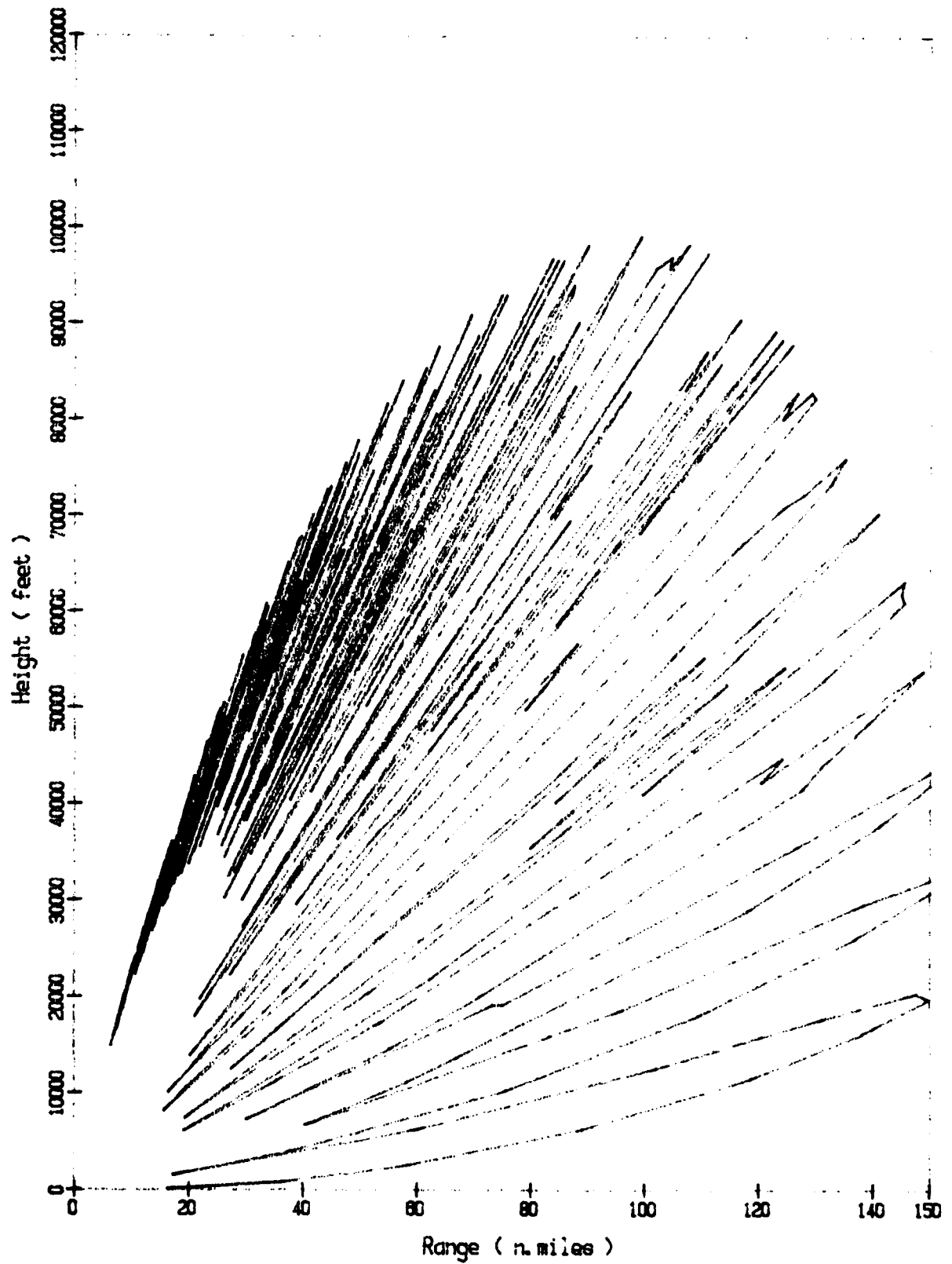


Figure 20. Simulation of effect of varying antenna height for UHF radar
Sea state : 3
Signal-to-noise : 0 dB
Antenna height fluctuation : $\pm 2.5\%$ of nominal height

DISTRIBUTIONCOPY NO.

Chief Defence Scientist	1
Deputy Chief Defence Scientist	2
CERPAS	3
SSPA	4
JIO (DSTI)	5
RANRL Library master copy	6
Counsellor, Defence Science, Washington	7
Defence Science Rep. London	8
Librarian Technical Reports Centre, Defence Central Library, Campbell Park	9
OIC Document Exchange Centre DISB	10 - 27
Flag Officer Commanding H.M. Australian Fleet	28
Director General, Naval Operational Requirements	29
Director of Tactics, AIO and Navigation	30
Director of Operational Analysis - Navy	31
Director of Surface and Air Weapons - Navy	32
Director of Electronic Warfare - Navy	33
Director of Radar Projects - Air Force	34
Director of Operational Analysis - Air Force	35
Director of Naval Aviation Policy	36
Director, Combat Data System Centre	37
Naval Scientific Adviser	38
Air Force Scientific Adviser	39
Officer-in-Charge RAN Trials and Assessing Unit	40
Director, RAN Tactical School	41
Joint Directors, Australian Joint Anti-Submarine School	42
Senior Librarian, Defence Research Centre Salisbury	43
Senior Librarian, Aeronautical Research Laboratories	44
Librarian H Block, Victoria Barracks, Melbourne	45
Dr M. R. Battaglia	46
Lt Cdr P. Williams, RAN	47
Dr J. L. Whitrow, Electronics Research Laboratory	48
RANRL Library	49 - 53

DOCUMENT CONTROL DATA SHEET

1. a. A.R. No. 003-419	1.b. Establishment No. RANRL Tech Note (External) 1/84	2. Document Date May 1984	3. Task No A3/83
4. Title The Calculation of the Radar Vertical Coverage Diagram		5. Security a. document UNCLAS b. title UNCLAS c. abstract UNCLAS	6.No Pages 45 7.No Refs 8
8. Author(s) BATTAGLIA, M.R.		9.Downgrading Instructions N/A	
10. Corporate Author and Address RAN Research Laboratory P.O. Box 706, Darlinghurst. N.S.W. 2010		11.Authority (as appropriate) a.Sponsor b. Security c.Downgrading d.Approval a. NAV b. HORD c.N/A (unclass) d.M.D.Frost, Director RANRL <i>M. D. Frost</i>	
12. Secondary Distribution (of this document) Approved for Public Release			
13. a. This document may be ANNOUNCED in catalogues and awareness services available to : No limitations			
13. b. Citation for other purposes (ie casual announcement) may be as for 13a.			
14. Descriptors Radar, model, multipath, clutter, attenuation, backscatter, probability of detection		15. COSATI Group 17090	
16. Abstract Algorithms are described for the calculation and plotting of radar vertical coverage diagrams. Two contour VCD algorithms are presented, with a brief discussion on the problem of numerical stability, and the effects of ship motion and frequency agility.			

Figure 9. Signal returns for UHF radar at constant elevation angle
of 7.0 and 7.35 degrees. Sea state 0.

END

FILMED

9-84

DTIC

Figure 17. Cont
Sea e
Signe
Algor

